INVESTIGATION OF PEO-POLYMER BLEND ELECTROLYTES FOR ELECTROCHEMICAL CAPACITORS

A thesis submitted to the Department of Materials Science and Engineering
African University of Science and Technology, Abuja

In partial fulfillment of the requirements for the degree of

MASTER OF SCIENCE

By

UBA, CHUKWUDALU UCHENNA

Supervised by

Dr. Abdulhakeem Bello

African University of Science and Technology www.aust.edu.ng

P.M.B 681, Garki, Abuja F.C.T Nigeria

July, 2019

APPROVAL PAGE

INVESTIGATION OF PEO-POLYMER BLEND ELECTROLYTES FOR ELECTROCHEMICAL CAPACITORS

By

Uba, Chukwudalu Uchenna

A THESIS APPROVED BY THE DEPARTMENT MATERIALS SCIENCE AND ENGINEERING

RECOMMENDED: _____

Supervisor: Dr. Abdulhakeem Bello

_____

Head, Department of Materials Science and Engineering

APPROVED: _____

Chief Academic Officer

_____

Date

CERTIFICATION

This is to certify that the thesis titled "***Investigation of PEO-Polymer Blend Electrolytes for Electrochemical Capacitors***" submitted to the Department of Materials Science and Engineering in the African University of Science and Technology (AUST), Abuja, Nigeria for the award of the Master's degree is a record of original research carried out by ***Uba, Chukwudalu Uchenna***.

ABSTRACT

Recently, there has been a drift of attention towards gel polymer based electrolytes owing to the fact that they are cheap and can achieve an extended potential window for improved energy density in supercapacitor devices when compared to aqueous electrolytes. Thus in this regard, the electrochemical characterization of symmetric supercapacitor devices based on different polyethylene oxide (PEO) based gel electrolytes was studied. The gel polymer electrolyte is based on methanol solvent, polyethylene oxide (PEO), lithium perchlorate ($LiClO_4$) and ionic liquid (IL), tetraethylammonium tetrafluoroborate ($TEABF_4$). Polymer electrolytes with different compositions were prepared by varying the weight percentage of each of the constituents. The EDLC device made with the electrolyte composition of PEO: 10 wt. % $LiClO_4$ + 20 wt. % IL showed a maximum operating voltage window of 2.3 V. A peak capacitance of 54.9 Fg^{-1}, energy and power density of 23.2 kWh g^{-1} and 10.8 kW/g were recorded. The enhanced performance were due to the improved conductivity of the electrolytes, which is favourable for fast ion transport.

ACKNOWLEDGEMENT

I am grateful to God almighty for his grace and strength, this project was a huge success because of your divine mercy and grace on me. To my supervisor Dr. Abdulhakeem Bello, if not for your encouragement, guidance and corrections, this project work would not be close to completion. I am indeed very grateful to you. I am also want to thank the Head of Department Prof. P. A. Onwualu not just for his fatherly advice and guidance throughout the duration of this project but also for his immeasurable contributions to my success in academics.

To the entire academic and non-academic staff of the African University of Science and Technology, I am grateful for your contribution towards my academic background and for your support throughout my duration of struggle.

Finally, I will not forget my lovely parents, Engr. Chris O. Uba and Mrs Ogugua P. Uba, for their unquantifiable and unending love, care and support; I am forever indebted to you. To my siblings, Mrs Ebele C. Metuh, Mr Obinna A. Uba and Miss Nneamaka Uba, I am most grateful for all your prayers, advice and support. To my friends, colleagues and well-wishers who in one way or the other directly or indirectly contributed to the success of this project work, I say a big a big thank you.

DEDICATION

I dedicate this work to the thesis to God, who endowed me with the grace and strength to accomplish this task.

TABLE OF CONTENTS

LIST OF FIGURES

LIST OF TABLES

CHAPTER ONE

INTRODUCTION

1.1 Background to the Study

In recent years, there has been an increasing enthusiasm in renewable energy due to the limitation of the available crude oil resources and the growing concerns about their negative environmental impacts. Migrating from fossil-derived energy to that stemming from renewable sources provides the avenue of green energy and simplifies energy distribution, by transmitting electrons over a grid or even by producing the energy from renewable sources on-site, as against translocating the fossil based fuels. However, energy derived from renewable sources, such as sunlight, wind, and tide, are short lived and therefore requires appropriate storage to ensure efficient, continuous, reliable and affordable energy supplies [1]. Different energy storage technologies have been developed for various applications, they include superconducting magnetic energy storage (SMES), capacitors, supercapacitors flywheels, batteries, pumped hydro storage, compressed-air energy storage (CAES) etc. [2].[3].

The rapid-growing market of portable electronics and electric vehicles triggers the development of environmental friendly energy storage devices that have high energy and power density, such as supercapacitors batteries. Although batteries possess much energy density, their relatively low power densities and poor life cycle limit their efficacy in high power demanding applications such as regenerative braking and load leveling systems. In comparison, supercapacitors have the ability to store much more amount of energy than the traditional dielectric capacitors and supply energy at a faster rate than batteries. Because of this, they are adapted for applications that require energy pulses in short periods of time, e.g., seconds or tens of seconds. Such exceptional properties stem from the nanoscale capacitors which are formed by the polarized electrode material and a layer of attracted ions from the electrolyte on its surface. The thickness of the electrode-electrolyte interface is directly proportional to the size of ions [4].

Supercapacitors (SCs), also named electrochemical capacitors (EC) and pseudocapacitors (PCs), are energy storage devices with excellent properties such as high power capability, excellent reversibility (90–95% or higher), and long cycle life (>105 cycles) have been studied over the past few decades. SCs working mechanism of is divided into two types: (1) electrical double-layer capacitors (EDLCs) and pseudocapacitors (PCs). In EDLCs, such as carbon based SCs, the capacitance stems from the charge separation at the electrode/electrolyte interface while in PCs, the capacitance arises from reversible faradic reactions occurring at the electrode surface, such as transition metal oxide based SCs [3]. They are widely employed in consumer electronics, as backup sources for memories, clocks, system boards, and microcomputers. SCs are also used as a short time energy storage device in fuel cell vehicles, hybrid electric vehicles, electric vehicles and industrial equipment, such as emergency power supplies in factories or hospitals, railway systems, airport buses, and for seaport rubber-tired gantry cranes [5][6].

1.2 Statement of Problem

Among the numerous electrochemical energy storage (EES) systems, the EDLCs have been depicted as one of the promising energy storage devices as they reflect favorable features of high energy density in comparison with conventional capacitors, predominant power density in comparison with batteries, fast charging-discharging rates, long cycling stability, and environmental friendly. All these summed up together, makes it possible for the EDLCs to yield unusually brilliant results in the next-generation energy storage systems [7]. In this regard, SCs are devices, which have gained much attention in recent years due to its broad range of applications in smart windows or intelligent displays etc. The limitation is that SCs have low energy density in relation to lithium ion batteries because of their electrochemical performances are usually limited by the electrode materials, electrolytes and their interactions. The most critical task in this area is to fabricate materials that are viable enough to serve as electrode or electrolyte materials and also have high mechanical strength, excellent capacitance, good conductivity and a large electrochemical window [8].

Prominently, the electrolytes used in electrochemical SCs determines the maximum operating voltage and safety of the device. Aqueous electrolytes, organic electrolytes etc. are the

conventional electrolytes, which are widely used in commercial EDLCs. They exhibit high ionic conductivities but however, have several issues ranging from easy leaking, carrying difficulty, high volatility, expansion through heat absorption, electrode corrosion to adapting a narrow temperature range [9]. In recent years, polymer electrolytes have attracted attention and suitable because they mirror not just excellent properties of safety and stability as well. Gel polymer electrolytes (GPEs) and micro-porous polymer electrolytes (MPEs) have recently garnered much attention due to the high ionic conductivity and timely safety (effective enough to preclude leakage in comparison with liquid electrolytes). Polyacrylamide (PAAM), polyethylene oxide (PEO) and polyvinyl alcohol (PVA)-based GPEs are examples of GPEs for EDLCs [7].

1.3 Aim and Objectives of the study

The aim of this work is to probe the suitability of a novel PEO-blend polymer electrolyte for electrical supercapacitor application through the following set of objectives:

- Mixing of polymer blend with a suitable ionic liquid to form the electrolyte.
- Characterization of the GPBE via Fourier transform infrared spectroscopy (FTIR).
- Electrochemical characterization of the SC devices fabricated using the GPBE via electrochemical impedance spectroscopy (EIS) and cyclic voltammetry (CV).

1.4 Scope of study

This work explores the possibility of a new PEO-polymer blend electrolyte for EDLC devices. The work targets the improvement of the electrochemical performance a PEO based polymer electrolyte by the addition of an ionic liquid and a conducting salt.

1.5 Organization

The five chapters in this project are in the following order;

- Chapter one, the introduction;
- Chapter two, the literature survey;
- Chapter three, the materials and methods;
- Chapter four, the results and discussion and
- Chapter five, consists of a summary and concluding remarks.

REFERENCES

[1] A. Noori, M. F. El-Kady, M. S. Rahmanifar, R. B. Kaner, and M. F. Mousavi, "Towards establishing standard performance metrics for batteries, supercapacitors and beyond," *Chem. Soc. Rev.*, vol. 48, 1272–1341, 2019.

[2] G. A. Tiruye, "Application of ionic liquids, innovative polymer electrlytes and novel carbonaceous materilas in supercapacitors," 2016.

[3] R. Zhang, "a Study of Flexible Supercapacitors: Design, Manufacture and Testing," no. June, 2016.

[4] Q. Gao, "Optimizing carbon/carbon supercapacitors in aqueous and organic electrolytes To cite this version : HAL Id : tel-00872080 Optimizing carbon/carbon supercapacitors in aqueous and organic electrolytes," 2013.

[5] R. Kotz and M. Carlen, "Principles and applications of Caps," vol. 45, pp. 1–16, 2000.

[6] J. R. Miller and P. Simon, "Materials science: Electrochemical capacitors for energy management," *Science* vol. 321, 651–652, 2008.

[7] N. Lu *et al.*, "High performance electrospun Li + -functionalized sulfonated poly(ether ether ketone)/PVA based nanocomposite gel polymer electrolyte for solid-state electric double layer capacitors," *J. Colloid Interface Sci.*, vol. 534, 672–682, 2019.

[8] S. A. Alexandre, G. G. Silva, R. Santamaría, J. P. C. Trigueiro, and R. L. Lavall, "A highly adhesive PIL/IL gel polymer electrolyte for use in flexible solid state supercapacitors," *Electrochim. Acta*, vol. 299, 789–799, 2019.

[9] D. Wang, L. Yu, B. He, and L. Wang, "A high-performance carbon-carbon(C/C) quasi-solid-state supercapacitor with conducting gel electrolyte," *Int. J. Electrochem. Sci.*, vol. 13, 2530–2543, 2018.

CHAPTER TWO

LITERATURE REVIEW

2.1 Energy Crisis of the World

There is no doubt that world economy, ecology, has been affected by climate change due to the gradual consumption of the fossil fuels, and green house emissions have become global objectives being essential for the sustainable development of economy and the society. Electricity production from the renewable energy sources and further improvement of energy efficiency are the most propitious and potential solutions for actualizing these objectives [1].

The United States Department of Energy (DOE) forecasts that twenty years from now, the world's energy consumption will surge by 20% (Figure 1.1), and that the growing global energy crisis. They stated that the energy crisis for the past two decades is attributed to the exorbitant cost of energy storage devices, reduction of natural resources, extreme ecological and environmental concerns, which are due to the consumption of fossil fuels, which, has ignited interest in the research, and development of sustainable energy development and the enhancement of renewable energy systems. With the critical role of energy storage devices in high power energy related applications, it has become imperative to actualize the future energy need by exploring alternative options for reliably low-cost energy storage devices [2]. Also, advances in energy storage and efficient power conversion systems that will increase the proficiency of global energy usage are vital in order to meet the daunting challenges of global warming and the finite nature of fossil fuels[10].

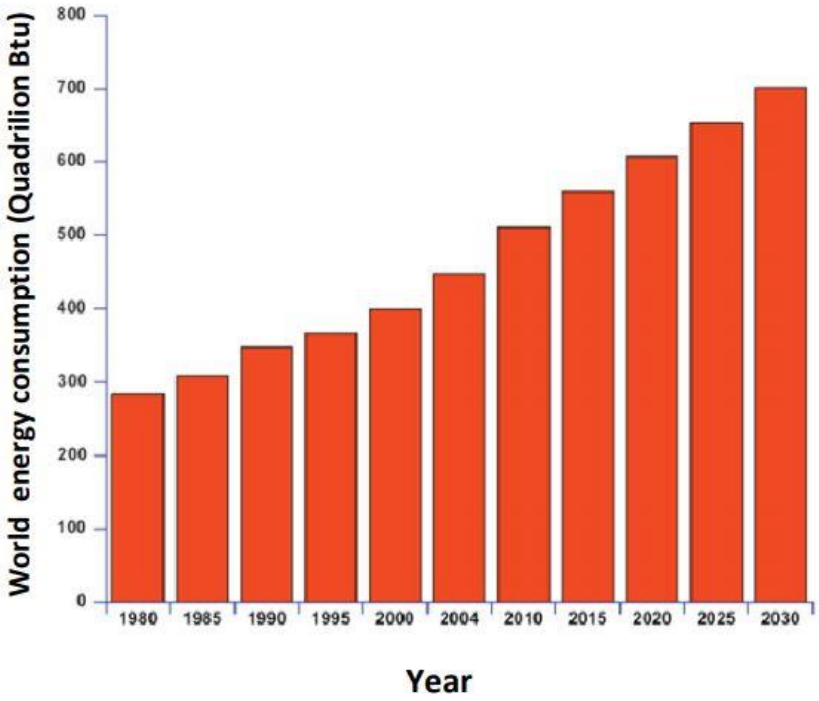

Figure 2. 1: The United States Department of Energy values and forecasts for energy utilization in the period from 1980 to 2030 [2].

Presently, there exists different varieties of electricity generating technologies that are still under development in a bid to thwart the dependence on the use of fossil fuels. These include solar, gas, biomass, tidal waves, hydro, wood waste, nuclear energy, sewage gas, solar thermal, landfill gas, geothermal and wind etc. [1]. However, the main drawback with renewable energy generation systems is that the electricity generated must be used immediately. Furthermore, implementation of renewable energy sources such as solar or wind energy pose difficulties to power management and grid stability. This is because of the large fluctuations in the generation of electricity from the actual energy demand. Hence, in other to meet the world's future energy goal, there is the need for the development of efficient energy storage [2]. Energy storage technologies can enhance the efficiency of supply systems by storing the energy when in great quantities and releasing it at a time of high demand [3]. Supercapacitor technologies are eco-friendly and can help in the development of more viable efficient systems through the knowledge of materials chemistry and materials engineering which specifically targets and improves the

nanostructured properties of electrode materials, thereby uplifting the electrochemical response at the electrode/electrolyte interface. Further material progression and breakthrough in research and development fundamentals, as well as engineering improvements, need to be amended so as to establish energy storage systems that will help pacify global energy storage and conversion impasses [2].

2.2 Electrochemical Capacitors: Theory and Operation

Supercapacitor (SC) has a capacity which is greater than that of the conventional capacitor [4]. The description of the working mechanisms for the conventional capacitors and SCs are as follows;

The conventional capacitor comprise of two conducting metals and in order to limit electrical contact between them, a dielectric is inserted between the two metals. When a voltage is applied, opposite charges accumulate on the surface of each electrode. The generated charges are separated by the dielectric as seen clearly in figure 2.2. [4].

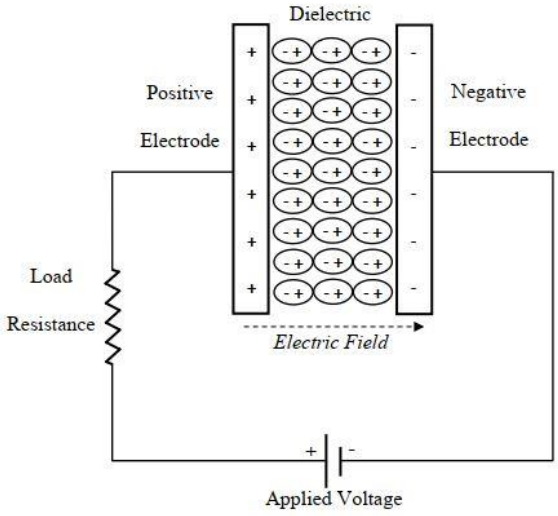

Figure 2.2: Schematic of a conventional capacitor [5]

Capacitance C (F) is the ratio of stored charge Q (Columb) to the applied voltage V (Volts):

$$C = \frac{Q}{V} \quad \text{... ... ...} \quad \textbf{(2.1)}$$

The capacitance (*C)* is calculated using the equation below

$$C = \varepsilon_0 \varepsilon_r \frac{A}{D} \quad \ldots \quad \ldots \quad \ldots \quad (2.2)$$

Where A represents the specific surface area of each electrode ($m^2 g^{-1}$), D is the distance between the two electrodes (m), ε_0 is the dielectric constant of free space (Fm^{-1}), and ε_r represents the dielectric constant of the insulating material between the two electrodes. The energy density and power density are two basic characteristics of a capacitor. The energy (E) of a capacitor is evaluated as follows:

$$E = \frac{1}{2} CV^2 \quad \ldots \quad \ldots \quad \ldots \quad (2.3)$$

The power P is the energy expended per unit time. As evident in Figure 2.2, in other to determine P for a capacitor, it becomes imperative to describe such a capacitor as a circuit in series with an external resistance R. The internal resistance is known as the equivalent series resistance (ESR). In other words, the internal components of the capacitor, such as electrodes, current collectors and dielectric materials, all contribute to the value of the ESR. The discharge current is a function of these resistances. Hence when the matched impedance ($R = ESR$) is measured, the maximum power P_{max} for a capacitor [4] can be calculated using equation 2.4:

$$P = \frac{V}{4 \times ESR} \quad \ldots \quad \ldots \quad \ldots \quad (2.4)$$

Equation (2.4) shows how the ESR can affect the maximum power of a capacitor. For a capacitor, the energy or power density is expressed as per unit mass or per unit volume. Conventional capacitors have relatively more power densities, but relatively, they have low energy densities in comparison to electrochemical batteries and to fuel cells as shown in Figure 2.3. In other words, a battery can store more energy than a capacitor, but it cannot deliver it very quickly, so its power density is low. Capacitors, on the other hand, store relatively less energy per unit mass or volume, but electrical energy stored can be discharged rapidly to produce a large power, so their power density is usually high.

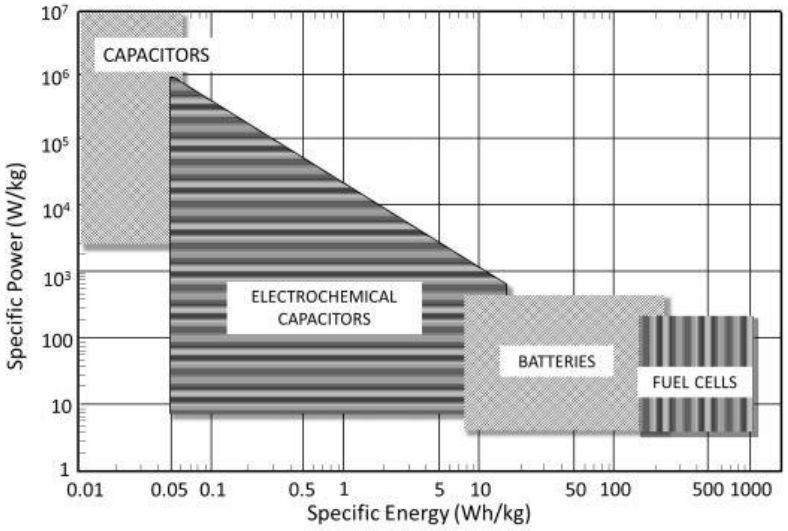

Figure 2. 3: Ragone plot for various energy storage and conversion devices. The indicated areas are rough guide lines [5]

Generally, the basic principle for conventional capacitors is also applicable for supercapacitors (SCs) as well. Evident from Figure 2.1 and Figure 2.4, the schematic representation of SCs and that of a conventional capacitor are quite similar. The SC device consist of two conducting electrodes that are separated by an insulating dielectric material. The disparity between the conventional capacitor and a SC is that the electrodes for SC device has a higher surface area than that of a conventional capacitor, the electrolyte solution and the separator between them. Therefore, with this effect, the capacitance and energy can be estimated from equations (2.2) and (2.3) [4].

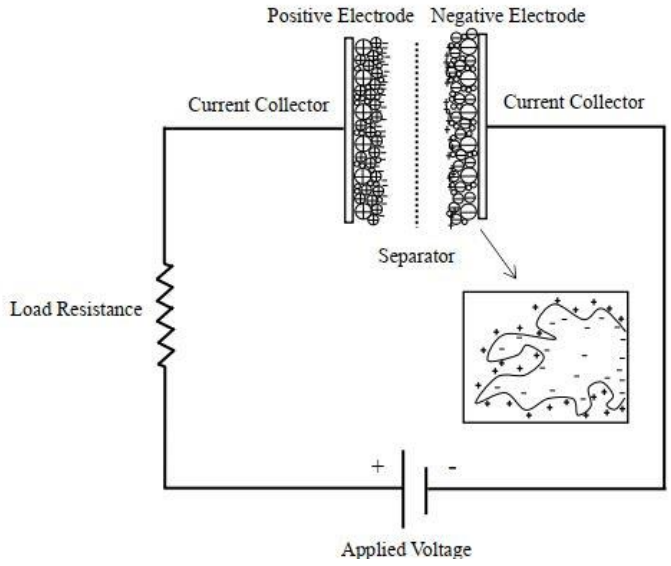

Figure 2.4: Schematic of an electrochemical double-layer capacitor [5]

2.2.1 Principle of Energy Storage

Electrochemical capacitors (EC) accumulate the electric energy in an electrochemical double layer (Helmholtz Layer) created at a solid/electrolyte interface. Positive and negative ionic charges within the electrolyte build up at the surface of the solid electrode and reimburse for the electronic charge at the electrode surface. The thickness of the double layer is a function of the concentration of the electrolyte and on the size of the ions and is in the order of 5 -10 Å, for concentrated electrolytes. The double layer capacitance is around 10–20 μFcm^{-2} for a smooth electrode in concentrated electrolyte solution and can be calculated according to equation (2.2). The combination of the two electrodes produces an electrochemical capacitor of high capacitance [6]. Figure 2.5 depicts a schematic diagram of an electrochemical double-layer capacitor comprising of a single cell possessing a high surface-area electrode material, which is loaded with electrolyte. The schematic representation also shows the potential drop across the cell.

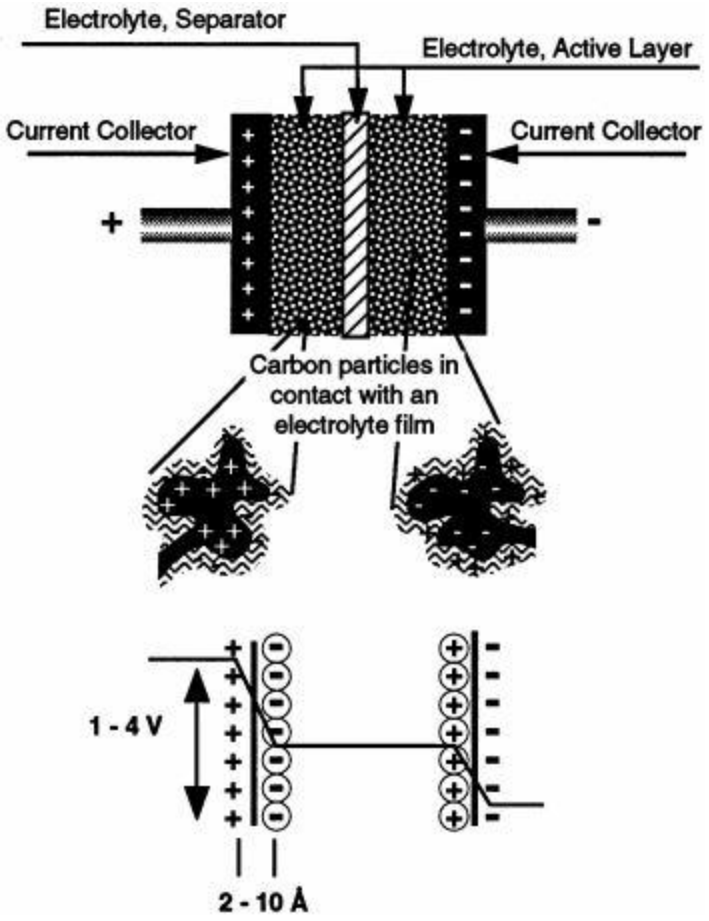

Figure 2.5 Principle of a single-cell double-layer capacitor and illustration of the potential drop at the electrode/electrolyte interface [6]

The capacitance of a single electrode can be calculated by assuming a high surface area carbon with 1000 m^2g^{-1} and a double layer capacitance of 10 µF cm^{-2}. This hints to a specific capacitance of 100 Fg^{-1} for one electrode. For a capacitor, two electrodes are desired with doubled weight and half the total capacitance ($C^{-1} = C_1^{-1} + C_2^{-1}$) resulting in 25 Fg^{-1} of active capacitor mass for this example. The difference between single electrode values and specifications given for the complete capacitor is of significant importance [6]. Whenever specifications of an EC are given, it should be indicated if the values correspond to a single electrode measurement or are deduced for a complete capacitor. The distinction between these two scenarios is a factor of four and therefore of substantial importance. The maximum energy stored in such a capacitor is given by equation 2.3.

2.3 Classification of Supercapacitors

Based on the working mechanism, SCs are divided into three: EDLCs, PCs and hybrid capacitors (HCs) (See Figure 2.6). The SCs show unique mechanisms for charge storage, which are reversible faradaic redox, electrostatic storage and a combination of the two. In PCs, there are faradaic processes that involve oxidation-reduction reactions. The energy stored in PCs is by a chemical mechanism, materials such as in transition metal oxide (TMOs) and PCs. Conversely, a non-Faradaic mechanism occurs in EDLCs, in which, the charges are kept apart at the electrode/electrolyte interface by physical processes such as carbon-based materials. The third type is the HC, the energy storage process is a combination of the faradaic and non-faradic process. Example of such are the carbon and transition metal oxide materials composite supercapacitors [8].

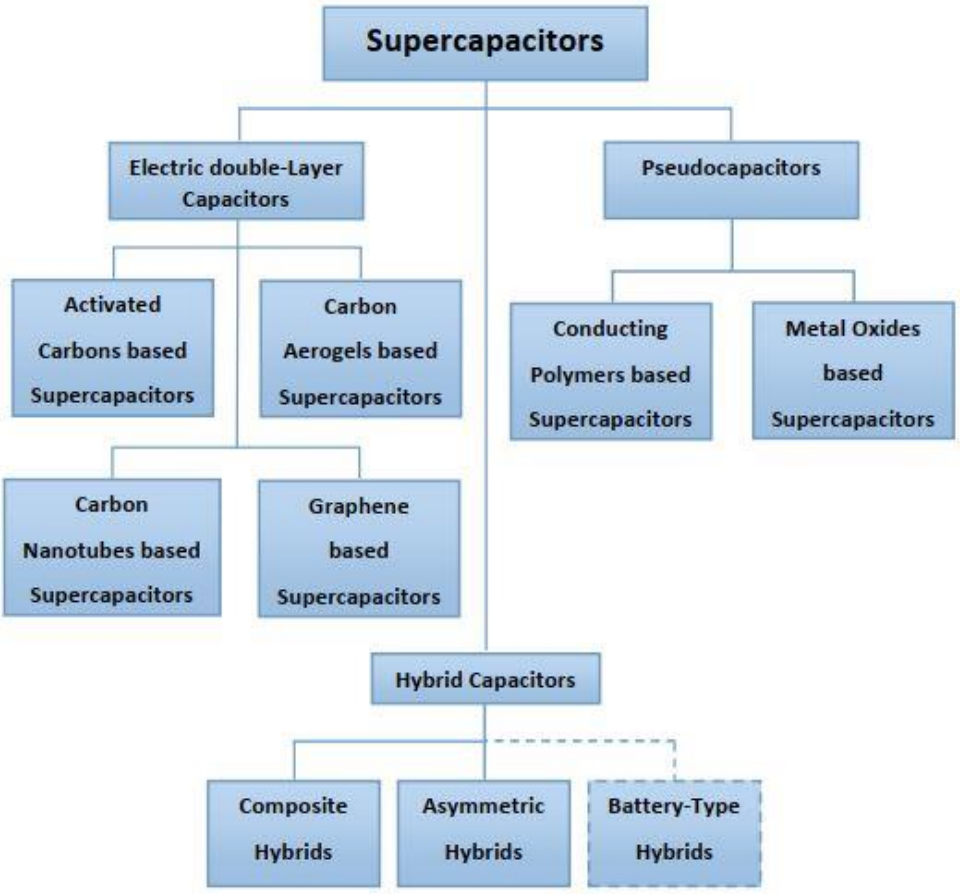

Figure 2.6: Classification of supercapacitors [5]

2.4 Electrochemical Testing of Cells

PCs SCs are able to deliver high rates of charge and discharge, they are limited for energy stored. The electrode material determines the capacity of PCs SCs and as a result, research to improve the performance of electrode materials has dramatically increased. While test methods for packaged PCs SCs are well developed, it is often impractical for the materials scientist to assemble full sized, packaged cells to test electrode materials. Methodology to measure a material's performance for use as an SC electrode is not standardized with various techniques yielding different results. The electrode material is a key component that determines an SC's capacity and the most definitive test for a new electrode material is how it performs in a full scale, commercial SC [9].

2.4.1 Fabrication of Electrodes for Testing

The electrode material is the heart of the SC device, which is the determinant of the electrochemical performance in terms of capacitance, self-discharge, life expectancy, resistance etc. As such, diligence and a painstaking attitude is required during the process of fabrication to obtain a high performing and durable electrodes. A highly conductive current collector is used as a base where the active material will be coated onto for testing.

The slurry/paste-like active material is made with a binder and a conductive additive (i.e. carbon black), the slurry is then uniformly coated onto the current collector and then placed in an oven to dry. The thickness of the electrode ranges from a few tens of micrometers to sub-millimeters. This being a function of the active material used and the proposed application. Furthermore, the mass of the active material under probe must be known and preferably its resultant volume. The as-obtained electrode is the "working electrode".

2.4.2 Electrochemical Testing of Electrode Material in a Three (3) and Two (2) Electrode Configuration

Methodology for electrode material testing can be grouped into test fixture configuration and measurement procedures [9]. Test fixture configuration includes the test fixture type along with guidelines for electrode mass and thickness, and other cell components including the electrolyte, separator, current collectors, and binder. Measurement procedures include electrochemical measurements and parameters along with the computations to reduce the data to the desired metrics [9].

2.4.2.1 Test Fixture Configuration

A typical SC unit cell is made up of two electrodes that are separated by a porous separator, often times, conductive and low surface area additives such as carbon black are added to enhance electrical conductivity. Current collectors of metal foil or carbon-filled polymers are utilized to conduct electrical current from each electrode. The separator and the electrodes are infused with an electrolyte, which permits ions to flow between the electrodes while inhibiting electronic

current from discharging the cell. A packaged SC module, irrespective of the desired size and voltage, is made of several repeating unit cells. A test fixture configuration that closely replicates the unit cell configuration will more closely match the performance of a packaged cell [9], [10].

Two-electrode test fixtures are either obtainable commercially or can be easily fabricated from two stainless steel plates as shown in Figure 2.7. Three-electrode electrochemical cells consist of a working electrode, a reference electrode and a counter electrode as shown in Figure 2.8. Three-electrode cells differ from two-electrode test and packaged cells in several important aspects. With the three-electrode configuration, only the working electrode contains the material analyzed and the applied voltage and charge transfer across the single electrode are markedly different than in the case of a two-electrode cell configuration. For a three-electrode cell, the voltage potential applied to the working electrode is that shown on the X-axis of the cyclic voltammogram (CV) chart (and on the Y-axis of the constant current diagram) and is with respect to the particular reference electrode used [9], [10]. In a symmetrical two-electrode cell, the potential differences applied to each electrode are equal to each other and are one-half of the value for a three –electrode cell set-up. Therefore, for a given potential range on the X-axis of a cyclic voltammogram (CV), the working electrode of a three-electrode cell has twice the potential range as is applied to the electrodes in a two electrode cell and this results in a doubling of the calculated capacitance value. The potential difference across the counter electrode in a three-electrode cell is neither controlled or measured, and is an order of magnitude or more lower (in the typical case that the counter electrode is larger than the reference electrode) or can be approximately equal (in the case that the working and counter electrodes are of the same size and material.) The point of zero charge location (PZC) on the CV also differs for each reference electrode/electrolyte/material combination and not unless the location is experimentally ascertained and used as the minimum voltage during a CV scan, the working electrode can really reverse polarizations during cell operation [9], [10].

The values obtained in a three-electrode cell configuration double those of the two-electrode cell configuration. The mass of the active material and thickness of the electrodes are factors which

also influence the measured results. Whether an ultracapacitor is fabricated to optimize energy density or power density, commercial cell electrode thicknesses range from about 10 mm thick (high power density) to several hundred microns thick (high energy density). Aside the fact that test electrodes should be of analogous thicknesses, extremely thin electrodes and/or which contain very diminutive amounts of material can lead to an exaggeration of a material's performance [9], [10].

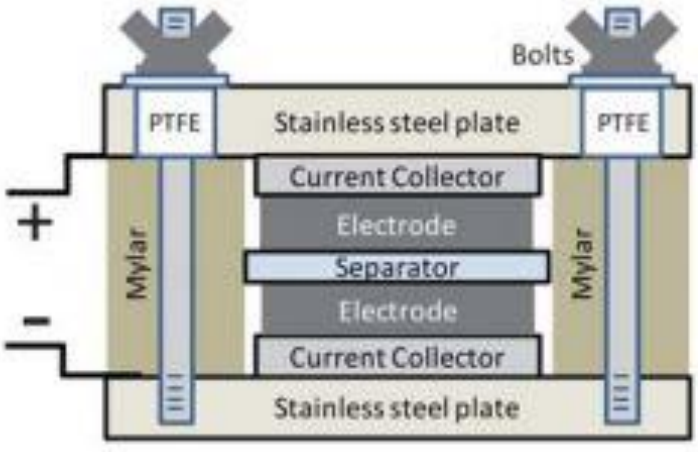

Figure 2. 7: Two-electrode test cell configuration [9]

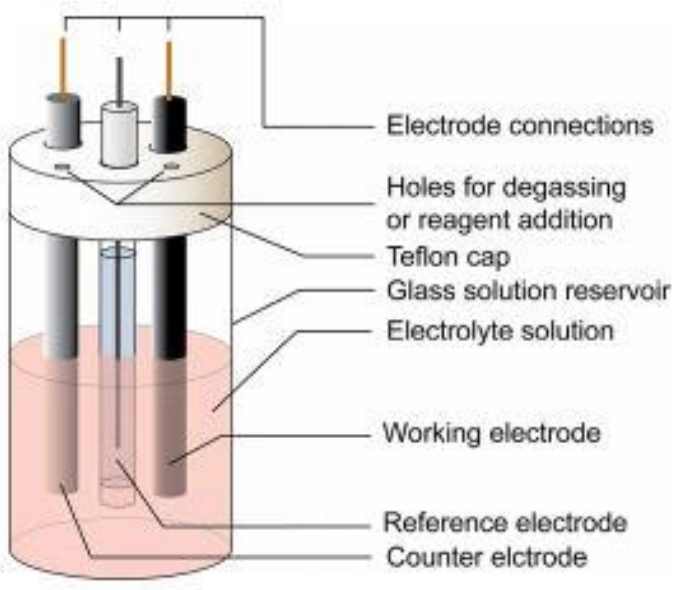

Figure 2. 8: Two-electrode test cell configuration [11]

2.4.2.2 Measurement Procedures

Charging rates, voltage ranges, and approaches for calculation of metrics also have an effect on the reported results and should replicate currently traditional and acknowledged techniques used for packaged cells. The prime performance metrics for packaged PCs SCs include gravimetric energy, power density, and life cycle testing. In a SC, the power scales with the square of voltage divided by its equivalent series resistance (ESR). The measured ESR of a test cell, as well as that of a full-scale packaged capacitor, is due to all cell components, which include leads, current collectors, electrodes, electrolyte, and separator. Therefore, only a fragment of the measured resistance are ascribed to the electrode material itself. Other metrics, such as an electrode material's energy and power density, also do not reveal a direct relationship to those of a packaged cell and must embrace information such as package dimensions and the mass of the other cell components to be meaningful [9].

Specific capacitance is the capacitance per unit mass for one electrode (equation (1))

$$C_{sp}(Fg^{-1}) = 4 \times \frac{C}{m} \quad \text{... ... ...} \quad \textbf{(2.5)}$$

Where C is the measured capacitance for the two-electrode cell and m is the total mass of the active material in both electrodes. The multiplier of 4 regulates the capacitance of the cell and the collective mass of two electrodes to the capacitance and mass of a single electrode. If volume is more imperative for the besieged application, the volume of the electrode material can be replaced for mass. Cell capacitance is best evaluated from galvanostatic or constant current (CC) discharge curves using equation (2) with I the discharge current and

$$C = I \Big/ \left(\frac{dV}{dt}\right) \quad \text{... ... ...} \quad \textbf{(2.6)}$$

dV/dt deduced from the slope of the CC discharge curve. Galvanostatic discharge is the recognized measurement method for ascertaining the capacitance value for packaged PCs in the

industry. This relates more closely to how a load is applied to the PC in most applications. The voltage range used for testing should be applicable to that which is used for commercial cells and should mirror the electrolyte's electrochemical window (from 0 V to approximately 1 V for aqueous electrolytes and from 0 V to 2.5–2.7 V for organic electrolytes). Maximum voltages for hybrid cells will be contingent upon electrode materials and electrolytes. The first portion of a discharge curve reveals an IR drop due to internal resistance while the rest of the curve will typically be linear for non-faradic materials. Pseudocapacitive and hybrid systems can showcase large deviations in linearity which are primarily based upon varying capacitance with voltage [9]–[11].

It is worthy to note that driving a cell above its true maximum operating voltage can result to an overestimation of specific capacitance. Cells operated at these levels will have truncated lifetimes and weak efficiencies because of the non-reversible reactions within the cell. Capacitance varies with voltage, especially for hybrid and Pseudocapacitive cells, and as such, it is pertinent to calculate the capacitance value using the typical operating voltage range for the application that the device will be utilized [9]–[11].

Most PCs will be operated in the range of V_{max} to approximately 0.5Vmax and the suggested method is to make use of two data points from the discharge curve with $dV/dt = (V_{max} - 0.5Vmax)/(T_2 - T_1)$. Including the lower half of the voltage range in the calculations can disrupt the seeming capacitance above that which is practically achievable for an actual application. Very low degrees of discharge also give rise to large amount of errors. This is especially when linked with small electrode masses, with the current from cell leakage, capacitance from other cell components, and faradic reactions supplying an increasing percentage of the indication as discharge rate. Using equation (2.6) and CV data, I is the average current during discharge (from Vmax to zero volts) and dV/dt, which is the scan rate. As with CC curves, capacitance depends on voltage range, scan rate, and computation method. Voltage scan rates of at least 20 to 40 mV s^{-1} are needed to uphold discharge times on the order of a minute and satisfactorily reflect a material's performance [9]–[11].

2.5 Evaluation of Devices

2.5.1 Cyclic Voltammetry (CV) and Cyclic Voltammetry Advanced (CVA)

Cyclic voltammetry (CV) is a degree of the current as a function of a predestined voltage range using a reversible linear voltage sweep known as the scan rate. The voltage applied between the two SC electrodes in the case of the two-electrode cells configuration and between a working electrode and reference electrode in the case of the three-electrode cell configuration. The potential in the CV starts at an initial voltage and rises linearly with respect to time until it attains a final voltage, the scan is reversed and the potential changes from the final voltage to the initial voltage at the same rate. The instantaneous current during the cathodic and anodic sweeps is noted to characterize the electrochemical reactions involved. The data are plotted as current (A) vs. potential (V) or sometimes as current (A) or potential (V) vs. time (s) [12]–[14]. To examine the charge storage mechanisms of supercapacitor materials where EDLC and PC types are typically apart, CV testing with the three-electrode setup is the most propitious technique. The test results is analyzed taking into account the shape of the resulting CV curve, which should be rectangular for EDLC. For some PC materials, pronounced redox peaks may occur in a highly reversible manner.

2.5.2 Electrochemical Impedance Spectroscopy (EIS)

Electrochemical impedance spectroscopy (EIS) is a very important technique to study the electrochemical performance of SCs. It measures the impedance of a power cell with respect to the frequency by applying a low-amplitude alternating voltage (normally 5 mV) which is superimposed on a steady-state potential. The resulting data are expressed in a Bode plot and in a Nyquist plot. While the Bode plot demonstrate the cell response between the phase angle and frequency, the Nyquist plot delineate the imaginary and real parts of the cell impedances on a complex plane. Aside the frequency response and the impedance, the EIS has also been used as a means to characterize the mass transport, charge transfer and charge storage mechanisms. It is used to estimate the capacitance, energy, and power properties. Different equivalent circuits and models developed to differentiate the contribution of individual structure component in a cell system to the total impedance of that particular cell. When SC devices are tested, the real parts

of the complex impedance at selected frequencies in literature to represent the ESR. However, one needs to keep in mind that this ESR obtained from the EIS test is often much smaller than that which is obtained from the constant current charge/discharge (CCCD) test.

2.6 Electrode Materials

In EDLC, no chemical reactions occurs for the storage of electrical charges but rather, energy is instead being stored through the adsorption of ions to the surface of charged electrodes. In pseudocapacitance, there occurs some ultra-fast redox reactions on the surface of the electrodes, increasing the energy density of the SC while decreasing its charge-discharge speed and its lifespan as well. The capacitance of a SC is dependent on the material used in the fabrication of the electrodes. In symmetrical SCs, there are two electrodes, which are made up of the same material. In asymmetrical, or hybrid SCs, there is often one electrode that exhibits PC, and a second corresponding that displays EDLC. This combination of the two types of capacitance is the sole reason why hybrid SCs maintain a better efficiency than standard pseudocapacitors, and a greater specific capacitance than EDLCs. There exists a surfeit of distinct materials that may be used in the electrodes of PC or the EDLC. Classic pure EDLCs typically employ electrodes produced of porous activated carbon (AC), but pseudocapacitors may also involve electrode materials such as transition metals and conducting polymers. There is no exact relationship between the increased specific surface area (SSA) of AC and capacitance, which is due to EDLC. But on the other hand, SSA is not the definitive contributor to capacitance, prompting research into different electrode materials [15], [16].

2.6.1 Carbon Materials

Carbon materials, in their various forms, are the most employed electrode materials in the fabrication of SCs. This is due its high surface area, low cost, availability and established electrode production technologies. Carbon materials employ the electrochemical double layer storage mechanism at the interface between the electrode and the electrolyte. The storage mechanism used by carbon materials is electrochemical double layer formed at the interface between the electrode and electrolyte. Hence, the capacitance principally depends on the surface area handy

to electrolyte ions. Vital factors, which affect electrochemical performance, are specific surface area, pore shape and structure, pore size distribution, surface functionality and electrical conductivity. The presence of large surface area in carbon materials, results in a high capability for charge accumulation at the interface of electrode and electrolyte. When rocketing specific capacitance for carbon materials, apart from pore size and high specific surface area, surface functionalization must be taken into consideration. Examples of carbon materials used as electrode materials are activated carbon, carbon nanotubes, carbon aerogels, graphene etc. [17], [18], [19].

2.6.1.1 Activated Carbon

The most widely used electrode material is activated carbon (AC) and this is a corollary of its large surface area, good electrical properties, well developed specific surface area (SSA) of up to 3000 $m^2 g^{-1}$ and moderate cost. AC can be produced either through the process of physical or chemical activation from numerous types of carbonaceous materials (e.g. wood, coal nutshell etc.). For the process of physical activation, carbon precursors are treated at high temperatures (700-1 200 ^oC) in the presence of oxidizing gases like steam, CO_2 and air. While in the case of chemical activation, the carbon precursors are treated at low temperatures (400 -700 ^oC) using activating agents such as sodium hydroxide, potassium hydroxide, zinc chloride and phosphoric acid. Porous structure of AC obtained via activation processes had a broad pore size distribution that consists of micropores (50 nm). Abundant researchers have tested the relationship between specific capacitance and specific surface area (SSA) of AC. Their reports shows what looks like a discrepancy between them. With a high SSA of around 3000 $m^2 g^{-1}$, a relatively small capacitance was obtained. This is a revelation that not all pores are effective during the process of charge accumulation. It is worthy to note that extreme activation causes an increase of the pore volume. This leads to draw backs like low conductivity and material density, which then results in a low energy density and loss of power capability [20]–[23].

2.6.1.2 Carbon Nanotubes (CNT)

CNT are used as SC electrode material because of its unique pore structure, good mechanical and thermal stability and superior electrical properties. CNTs are produced through the process of

catalytic decomposition of some hydrocarbons. By carefully tweaking different parameters, it becomes possible to manufacture nano structures in various conformations and control their crys talline structure. Unlike other carbon-based electrodes, CNTs permits a continuous charge distribution that uses almost all of the accessible surface area. CNTs possess a lower ESR than AC because the electrolyte ions can diffuse into the mesoporous network. They also additionally provide a good support for active materials as a result of their high mechanical resilience and open tubular network. Generally, CNT have small SSA (less than $500 m^2 g^{-1}$) which leads to a low energy density as compared to AC [22], [24]–[26].

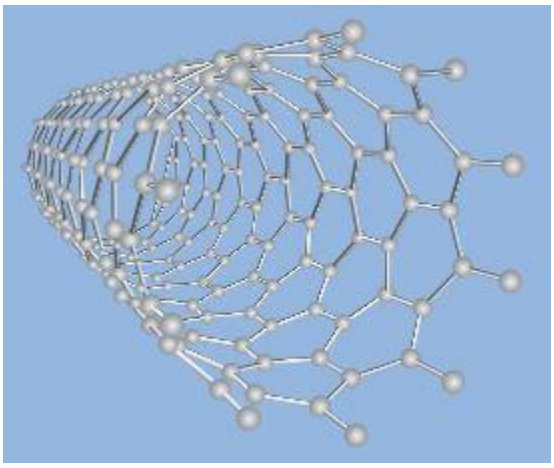

Figure 2.9: Structure of a single walled carbon nanotube [27]

2.6.1.3 Carbon Aerogel Derived from Biomasses

Carbon aerogel is another form of carbon, which is used as materials for SC electrodes, whereby the porous carbon is produced through pyrolysis of organic aerogels. The porosity is due to the blending of interconnected colloidal particles. The porous carbon materials could be composites, monoliths, powders, microspheres, or thin films. The aerogels carbon materials have been reported to exhibit higher surface area in comparison to AC. Carbon fiber aerogels with surface areas ranging from 1536 to 2436 $m^2 g^{-1}$ and pore size ranging between 1.0 and 4.0 nm exhibited high specific capacitance of 282 F g^{-1} (1 A g^{-1}) in 6 M KOH electrolyte [22], [28].

2.6.1.4 Graphene

Graphene is a material with a one-atom thick layer 2D structure. It has emerged as an exceptional carbon material that has prospect for energy storage applications because of its excellent characteristics of high electrical conductivity, chemical stability, and large surface area. Graphene is vaunted as a viable material for SC applications, because when graphene is used as electrode material it depends not on the distribution of pores at solid state, in comparison to other carbon materials such as AC, CNT etc. Graphene, which is newly developed, has higher SSA around 2630 $m^2 g^{-1}$. It is capable of achieving a capacitance of up to 550 F g^{-1} if the entire SSA is utilized. Another advantage of using graphene as electrode material is that both key surfaces of graphene sheet are exterior and are readily reachable by electrolyte. Methods of producing graphene include: chemical vapor deposition, micromechanical exfoliation, arch discharge method, unzipping of CNTs, epitaxial growth, electrochemical and chemical methods and intercalation methods in graphite [29]–[33].

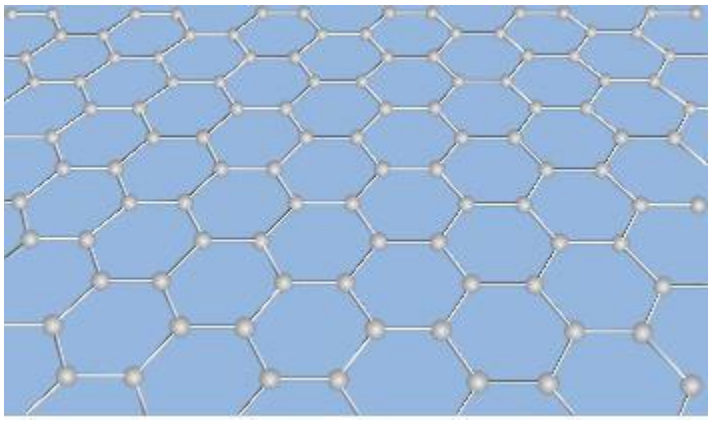

Figure 2.10 Structure of a graphene layer [27]

2.6.2 Conducting Polymers

Conducting polymers exhibit a relatively high conductivity and capacitance and ESR in comparison with carbon based electrode materials. There exist different electrode configurations that can be used for conducting polymers but the n/p type configuration, having one negatively charged (n-doped) and one positively charged (p-doped) electrodes, provides a high energy and power

densities, although due to the lack of n-doped, conducting polymer electrode materials have restricted PCs from reaching their potential. In conducting polymers, the process of charge storage and release is due to a reduction-oxidation process. Through the process of oxidation, also known as doping, ions are transferred to the backbone of the polymer whereas through the process reduction, also known as de-doping, ions are released back into the solution. On the other hand, this reduction-oxidation process in conducting polymers causes mechanical stress which thwarts the stability through many charge-discharge cycles. Taking into consideration the different types of conducting polymers, polyaniline (PANI) is the most auspicious SC electrode material because of its high conductivity, easy method of synthesis, excellent capacity for energy storage and excellent cost effectiveness. Its drawback is because through the repetitive cycles (charge/discharge process) swelling and shrinking occurs, and a rapid degradation in performance is evident. To ameliorate this, it is necessary to combine PANI with carbon material. When this is done, its stability is reinforced and its capacitance is maximized [4], [34]–[37].

2.6.3 Transition Metal Oxides and Hydroxides

Metal oxides present another substitute for materials used in electrodes fabrication SC. This is because they exhibit high specific capacitance and low resistance, thus making it simpler to fabricate SCs with high energy and power. The frequently used metal oxides are as follows: nickel oxide (NiO), ruthenium dioxide (RuO_2), manganese oxide (MnO_2), iridium oxide (IrO_2). They are feasible alternative because of their lower cost of production and use of a milder electrolyte. RuO_2 in both amorphous and crystalline is an important compound due to its unique combination of characteristics, like catalytic activities, metallic conductivity, electrochemical reduction-oxidation properties, high chemical and thermal stability and field emitting behavior. Its application include electronics, thick or thin resistors, ferroelectric films and integrated circuit development. The most current application of RuO_2 is as an electrode material in SCs due to the advantages it offers which include; long cycle life, wide potential window of high specific capacitance, highly reversible reduction-oxidation reaction, and metallic type conductivity.. Manganese oxide has recently enticed a lot of research interest because of its unique physical and chemical properties (its low cost, excellent capacitive performance in aqueous electrolytes

and environmental benignity). Its wide range of applications include: ion exchange, catalysis, biosensor, energy storage and molecular adsorption [38]–[43].

The electrode of a SC device must have a high specific capacitance in other to have a high electrochemical performance. In contrast with an EDL material, the favorable pseudocapacitive materials can attain higher specific capacitance. Prepared by the different methods, layered transition metal hydroxides have a range of flower-like lamellar structure. The hydroxides display high specific area and dedicated channels, which expedite for redox reaction towards actualizing high electrochemical behavior. The revealed tremendous pseudocapacitive performance makes them particularly suitable as electrode materials for SCs as they can exhibit smart pseudocapacitive performance. During their use as electrode materials, a reversible redox reaction occurs during the charge-discharge process. A high-performing electrode must meet the needs of high specific capacitance, high rate capacity and long stability [44]–[48].

2.6.4 Composites

Composite electrodes combine carbon-based material with either metal oxide or conducting polymer materials. The effect of this is that it in turn offers both physical and chemical charge storage mechanism together in a single electrode. Composite electrode materials for SCs include carbon-carbon composites, carbon-metal oxide composites and carbon-conducting polymer composites. In carbon-polymer based composites, conducting polymers such as polyaniline, polythiophen and polypyrrole with pseudo-capacitance properties are embedded in carbon nanomaterials (carbon fibre, MWCNT, fullerene and graphene) which have electrical double layer capacitance properties. In carbon-metal oxide based composites, carbon material because of its high surface area and regular pore structures is merged with metal oxides (like RuO_2, MnO_2 and Fe_2O_3) very easily, and also the carbon material has both ionic and electronic conductivity of the electrode surface. The resulting composite material thus exhibits high density and stable power densities. The incorporation of metal oxides with conducting polymers give rise to metal oxide-polymer based composites. This is done to enhance their electrochemical properties. Amongst

these transition metal oxides, hydrous ruthenium oxide has the best electrochemical properties than other transition metal oxides [26], [49]–[53].

2.7 Electrolytes

Electrolytes are one of the most significant components in the performance of electrochemical SCs, which include electrical double-layer capacitors, pseudocapacitors and hybrid supercapacitors. These electrolytes constitute ions for charge transport and storage. Since the energy density of SC device is proportional to the capacitance and the square of the voltage (refer to equation 2.3). To increase the energy density, either the capacitance or the cell operating voltage has to be increased [54]–[56].

Widening the potential window of an electrolyte i.e., enlarging the cell voltage (V), can effectively increase the energy density as seen from equation of 2.3. Increasing the cell voltage is more efficient than increasing the electrode capacitance in terms of energy density; this is because the energy density is directly proportional to the square of the cell voltage. Therefore, improving new electrolytes/solutions with broad potential windows should be given priority than the development of new electrode materials. Aqueous based SCs usually have an operating potential window of about 1.0–1.3 V because the aqueous electrolyte's potential window is about 1.23 V. The organic electrolyte and ionic liquid (IL) based SCs generally have potential windows of 2.5–2.7 and 3.5–4.0 V, respectively. Furthermore, electrolytes/solutions also play a crucial role in determining other important properties such as the power density, rate performance, internal resistance, cycling lifetime, operating temperature range, self-discharge and toxicity, (as seen in Figure 2.8) which are also key in the practical use of SCs [54]–[56].

The contact between the electrolyte and the electrode materials also plays an important role in the performance of the device, i.e. the exact fit between the electrolyte ion size and the pore size of carbon electrode material has a weighty stimulus on the achievable specific capacitance. The PCs obtained from the carbon-based materials and TMOs are greatly contingent to the nature of the electrolytes. The ionic conductivity of electrolytes plays a substantial role in the internal

resistance of the device especially for the case of organic and ionic liquid (IL) electrolytes. The viscosity, boiling point and freezing point of the electrolyte can also mainly influence the thermal stability and thereby the operating temperature range of the device. As identified, the aging and breakdown of devices are related to the electrochemical degradation of the electrolytes. With respect to the development of electrolyte for SC devices, a large variety of electrolytes such as aqueous electrolytes, organic electrolytes, IL electrolytes, redox-type electrolytes and solid or semi-solid electrolytes have been investigated and great advancement has been recorded during the past several decades [54]–[56].

Generally, the perquisites for a standard electrolyte are as follows: wide potential window; high ionic conductivity; high chemical and electrochemical stability; high chemical and electrochemical inertness to other SC components (e.g., electrodes, current collectors and packaging); wide operating temperature range; well-matched with the electrolyte materials; low volatility and flammability; environmentally friendly; and cost effective. Actually, it is almost impossible for an electrolyte to meet all of these requirements, and each electrolyte has its own merits and demerits.

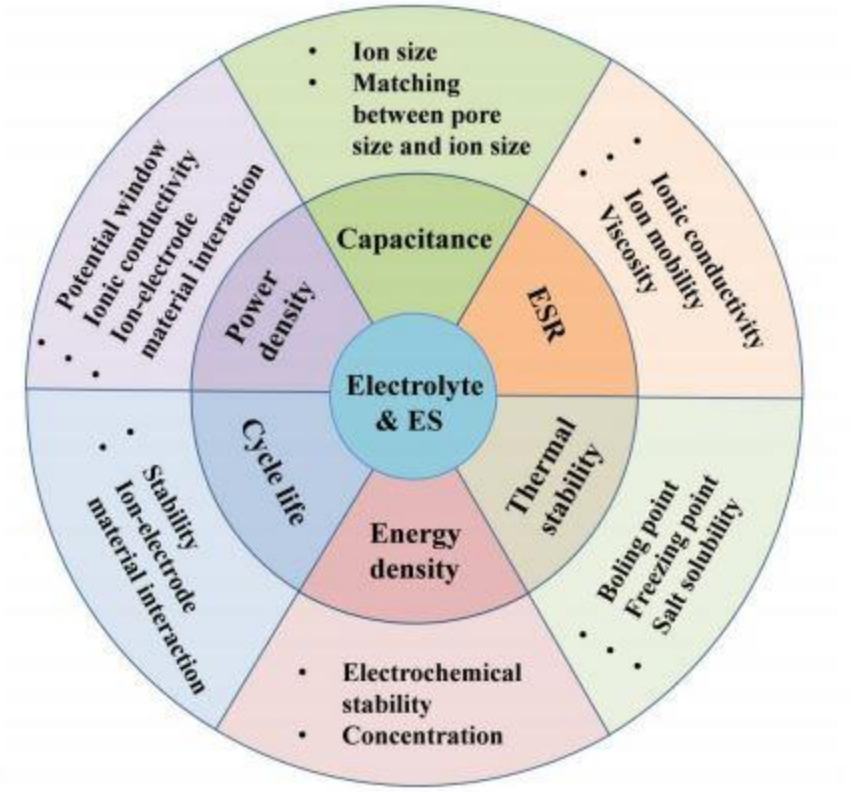

Figure 2. 11: Effects of the electrolyte on the electrochemical supercapacitor (ES) performance [54]

In general, different types of electrolytes have been established and reported in the literature to date. As shown in Figure 2.9, these electrolytes are categorized as liquid electrolytes and solid/quasi solid-state electrolytes. In general, liquid electrolytes classified into aqueous electrolytes, organic electrolytes and ion-liquids (ILs), while solid or quasi-solid state electrolytes can be divided into organic electrolytes and inorganic electrolytes. To date, there exists no ideal electrolyte developed, meeting all the requirements discussed previously [54]–[56].

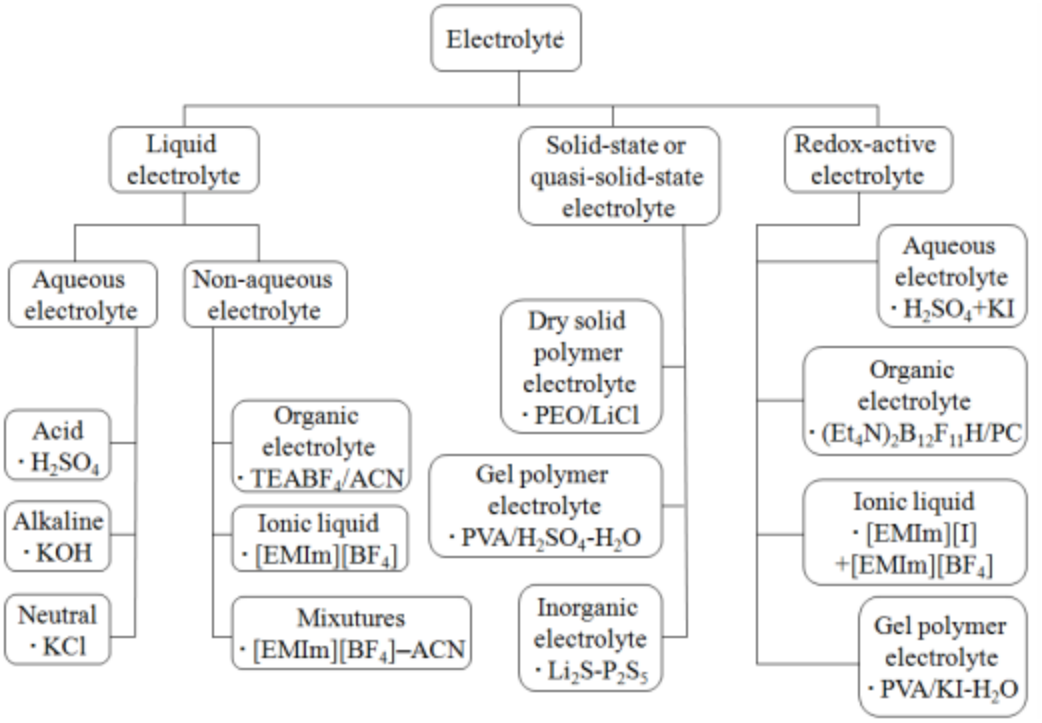

Figure 2. 12: Classification of electrolytes for electrochemical supercapacitors [54]

2.7.1 Aqueous Electrolytes

Aqueous electrolytes have a high conductivity value (for example, about 0.8 S cm^{-2} for 1 M H_2SO_4 at 25°C), which is at least one order of magnitude higher than that of organic and IL electrolytes. This is advantageous for lowering the ESR of the cell device, leading to a better power delivery of such device. The selection yardstick for aqueous electrolytes generally takes into consideration the sizes of bare and hydrated cations and anions and flexibility of ions, which affects not only the ionic conductivity but also the specific capacitance value. In addition, an electrolyte's ESPW and the corrosive intensity should be considered. In general, aqueous electrolytes can be classified into acid, alkaline, and neutral solutions in which H_2SO_4, KOH and Na_2SO_4 are respective representatives and the most often used electrolytes (Figure 2.11). As stated above, the main short coming of aqueous electrolytes is their relatively narrow ESPW, restricted by the decomposition of water [54], [57]–[63].

2.7.2 Organic Electrolytes

Organic electrolyte-based SCs are presently leading the commercial market due to their high operation potential window typically in the range of 2.5 to 2.8 V. The increased operation cell voltage can land a drastic improvement in both the energy and power densities. Furthermore, using organic electrolytes permits the use of cheaper materials such as aluminum for the current collectors and packages. Normal organic electrolytes for the commercial EDLCs consist of the conductive salts (e.g., tetraethylammonium tetrafluoroborate ($TEABF_4$)) dissolved in the acetonitrile (CAN) or polypropylene carbonate (PC) solvent [54], [62], [64]–[69].

However, there are other issues that should be taken into consideration when using the organic electrolytes for SCs. Compared to devices which use aqueous electrolytes, devices using organic electrolytes usually have a higher cost; have smaller specific capacitance; lower conductivity; and safety concerns related to the flammability, volatility and toxicity also raises an eye brow. Furthermore, organic electrolyte requires a convoluted purification and assembling processes under controlled environment to preclude any residual impurities (e.g., water) that can give rise to large performance degradation and serious self-discharge issues. Also, similar to aqueous electrolyte-based supercapacitors, the nature of salts and solvents, such as ion size, ion-solvent interaction, conductivity, viscosity and ESPW, has intense influences on the performance of organic electrolyte-based SCs [54], [62], [64]–[69].

Generally, organic electrolytes have bigger solvated ion sizes and lower dielectric constants, which can lead to lower EDL capacitance values. Therefore, it is vital to match the pore size of carbon materials with the size of electrolyte ions to amplify the specific capacitance. The degradation is because of the following reasons: (1) Broad operation cell voltage could accelerate the oxidation of electrode materials. This happens when the operating voltage of the device is higher than the typical values of 2.5–2.8 V such as above 3 V. This could lead to gas evolution due to the electrolyte decomposition and carbon electrochemical oxidation. (2) The electrolyte ion intercalation or the electrochemical reaction of the organic electrolytes could also lead to the degradation of the performance of the device; and (3) finally; harsh working conditions (e.g., high

peak temperature and working voltage) may trigger the degradation of the device performance. Therefore, understanding the aging and failure mechanisms will be beneficial to the development of devices with wider voltage windows. Another setback of organic electrolytes is their much lower ionic conductivity in comparison to the aqueous electrolyte. For example, the ionic conductivity of the commonly used 1 M $TEABF_4$/ACN electrolyte is 0.06 S cm^{-1}, which is significantly lower than that of the 30 wt. % H_2SO_4 electrolyte (0.8 S cm^{-1} at 25°C). The low conductivity of the organic electrolyte can result in a much higher ESR compared to the aqueous electrolyte-based ESs, which then thwarts the maximum power density [54], [62], [64]–[69].

2.7.3 Ionic Liquids

Ionic liquids are also known as low temperature or room temperature molten salts. ILs are salts, consisting cations and anions with melting point below 100 °C. An IL usually is composed of a large asymmetric organic cation and an inorganic or organic anion. This special combination of certain cation and anion provides to a low melting point. Due to their unique structures and properties, ILs have received much interest as alternative electrolytes for SCs. In general, ILs have several potential advantages including high thermal, chemical and electrochemical stability, negligible volatility, and non-flammability (depending on the combination of cations and anions). The physical and chemical properties of ILs can be highly tunable customized to meet certain requirements of ES performance such as operative cell voltage, working temperature range, ESR (related with the ionic conductivity), and so on due to their large variety (virtually unlimited) of combinations of cations and anions [54], [70].

ILs are classified as aprotic, protic and zwitterionic types based on their composition (Fig 2.12). The regularly used ILs for SCs in imidazolium, pyrrolidinium, ammonium, sulfonium, phosphonium cations, and so on. Typical anions of ILs are tetrafluoroborate ($BF4^-$), hexafluorophosphate ($PF6^-$), bis(trifluoromethanesulfonyl)imide ($TFSI^-$), bis(fluorosulfonyl)imide (FSI^-), and dicyanamide (DCA^-) [54].

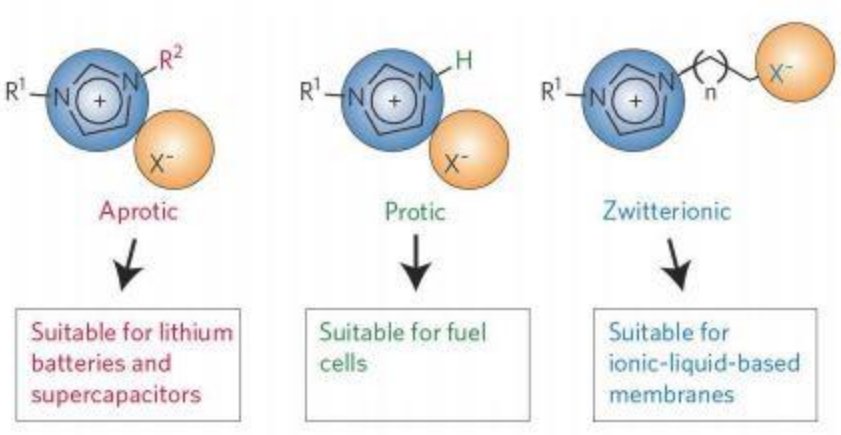

Figure 2. 13: Basic types of ionic liquids: aprotic, protic and zwitterionic types [54]

In general, the pyrrolidinium-based ILs have a wider ESPW while the imidazolium-based ILs can produce higher ionic conductivity. As stated before the operative cell voltages of commercial organic electrolytes (e.g., ACN and PC) based EDLCs are generally limited to 2.5–2.8 V, and increasing the cell voltage beyond this limit would cause serious electrochemical decomposition of organic solvents. However, many studies using IL- electrolyte-based SCs could give operative cell voltages above 3 V. Besides, commercially used organic solvents (e.g., ACN) also face safety issues due to their volatile and flammable nature especially when used at high temperatures. Solvent-free ILs may have an upper hand in attending to the safety problems associated with the use of commercial organic solvents, making IL-based SCs advantageous for high-temperature applications [71]–[73].

Unfortunately, the main drawbacks with most ILs are high viscosity, low ionic conductivity and high cost. These setbacks can limit their practical applications in devices. Even for [EMIM][BF4] electrolyte, which has a relatively high ionic conductivity among the common ILs, its conductivity (14 mS cm^{-1} at 25 °C) is still much lower than that of the $TEABF_4$/ACN (59.9 mS cm^{-1} at 25 °C). With the use of ILs in SCs devices, the rate and power performance are limited which in turn leads to a loss of the power density. This is because both the low conductivity and high viscosity of IL-based electrolytes can greatly increase the ESR values (which cannot be buffered by increasing of the cell voltage) of the IL based devices. In addition, the specific capacitance of IL electrolyte-

based EDLC devices are often less than those of both based on aqueous and organic electrolyte especially at high scan rates or high charging/discharging rates. This is probably due to the high viscosity of ILs. In order to understand the aging or failure mechanisms of IL electrolyte-based EDLCs, the electrochemical decomposition of ILs beyond the ESPW have been investigated by using instrumental analysis methods such as in-situ infrared and electrochemical spectroscopy methods and in-situ XPS [71], [74]–[76].

2.7.4 Solid- or Quasi-Solid-State Electrolytes for ESs

The rapid growing demand of power for portable electronics, wearable electronics, microelectronics, printable electronics and especially flexible electronic devices has placed the research and development spotlight on solid-state electrolyte-based electrochemical energy devices. The solid-state electrolytes can both serve as the ionic conducting media and as an electrode separator. The main merit of solid-state electrolytes are the simplification of packaging and fabrication processes of SCs and liquid-leakage free. Most of the solid-state electrolytes developed for SCs are polymer electrolytes only very limited work has dwelled on inorganic solid materials. The polymer-based solid electrolytes for SCs can be classified into three types: the gel polymer electrolyte which are also called quasi-solid-state electrolyte due to the presence of a liquid phase (GPE), the solid polymer electrolyte (SPEs, also known as dry polymer electrolytes), and the polyelectrolyte [77], [78].

Consider Figure 2.12, the SPE is comprised of a polymer (e.g., PEO) and a salt (e.g., LiCl), devoid of any solvent e.g. water. The ionic conductivity of SPE due to the translocation of salt ions through the polymer. On the other hand, the GPE is a polymer host (e.g., PVA) and an aqueous electrolyte (e.g., H_2SO_4) or a conducting salt dissolved in solvent. In this case, the polymer serves as a matrix, which is engulfed by the solvent. The ion transportation occurs in the solvent instead of in the polymer phase, which is quite distinct from that of the SPE. In the polyelectrolyte category, the ionic conductivity is supplied by the charged polymer chains [54].

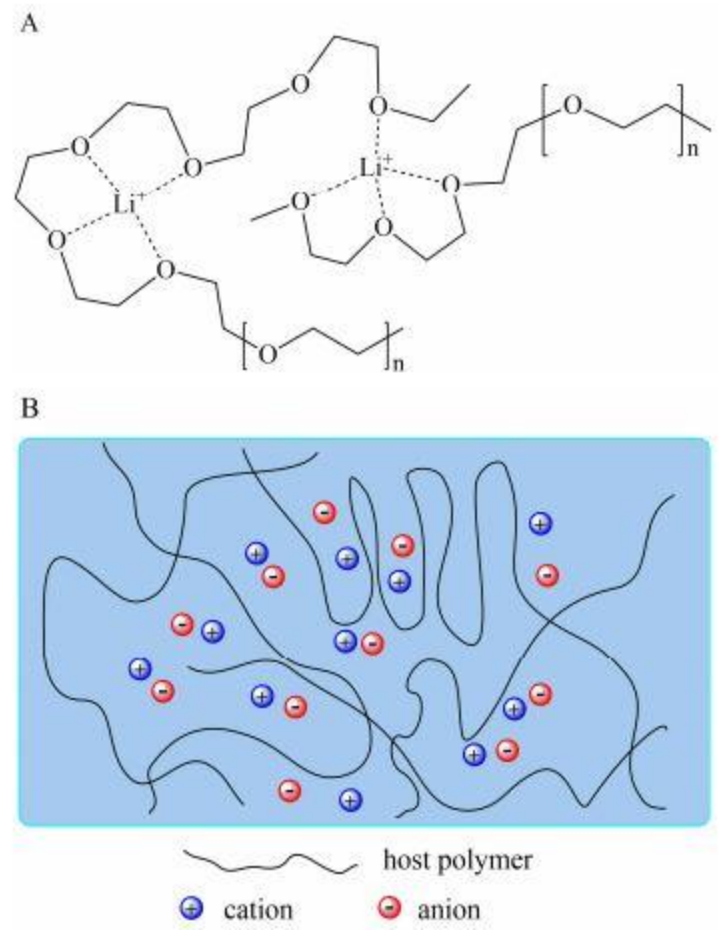

Figure 2. 14: Schematic diagrams of (a) dry solid-state polymer electrolyte (e.g., PEO/Li^+), (b) gel polymer electrolyte, and (c) polyelectrolyte [54]

Generally, GPEs have the highest ionic conductivity amidst these three categories of solid-state electrolytes. The presence of a liquid phase in a GPE, significantly raises its ionic conductivity higher than that of the dry SPE. This is the reason for its dominance in solid electrolyte-based supercapacitor products. GPEs may however, suffer from relative poor mechanical strength and narrow operative temperature range especially when water is the solvent. The weak mechanical strength of GPEs is another setback which is of main concern as it may lead to internal short circuits bringing about safety issues [79], [80].

Although dry SPEs normally have low ionic conductivity values, they have a relatively higher mechanical strength in comparison to GPEs. These solid-state electrolytes for SCs have a common disadvantage is a limited contact surface area between the solid electrolyte and the electrode material especially for nanoporous materials. This problem increases the ESR value, reduces the performance rate and limits the utilization of active electrode materials, which then result in a low specific capacitance of the device. Solid electrolytes are been used for various types of SCs such as EDLCs, PCs and hybrid SCs with different kinds of electrode materials. When developing solid-state electrolytes for SC application, the following requirements should be considered: (1) high chemical, electrochemical and thermal stability, (2) high ionic conductivity and (3) sufficient mechanical strength and dimensional stability. The reality is such that it is almost impossible for a solid-sate electrolyte to meet all of these requirements. There are often some trade-off between mechanical strength and ionic conductivity [81], [82].

2.7.4.1 Gel Polymer Electrolytes

GPEs are currently the most widely studied electrolytes for solid-state SCs due to their high ionic conductivity. GPE is made up of a polymer matrix (host polymer) and a liquid electrolyte (e.g., aqueous electrolyte, organic solvent containing conducting salt and ionic liquid). Some already explored polymer matrices for preparing GPEs are as follows poly(vinyl alcohol) (PVA), poly(-acrylic acid) (PAA), potassium polyacrylate (PAAK), poly (ethyl oxide) (PEO), poly(methylmethacrylate) (PMMA), poly(ether ether ketone) (PEEK), poly(acrylonitrile)-block-poly(ethylene glycol)-block-poly(acrylonitrile) (PAN-b-PEG-b-PAN), and poly(vinylidene fluoride-

co-hexafluoropropylene) (PVDF-HFP). A hydrogel polymer electrolyte results when water is the plasticizer. Hydrogel polymer electrolyte has three-dimensional polymeric networks can trap water in the polymer matrices mainly through surface tension. One of the most noteworthy advantages of using solid-state electrolytes including inSCs is because it permits the development of malleable structures and tunable shapes for different desired applications. For example, based on the PVA-based hydrogels, various solid-state have been developed, including flexible , stretchable , flexible micro-, printable micro-, on chip micro-,3D micro-, yarn, wire or fiber-shaped, transparent, ultrathin and weaveable SCs with other devices [54], [80], [81].

2.8 Prior Works on Gel Polymer Based Electrochemical Capacitors

A flexible GPE film with high conductivity based on green biopolymer-carboxylated chitosan was developed by Hezhen Yang et. al. [83] via the solution coating and crosslinking by hydrochloric acid for all-solid-sate SCs. For the preparation of the carboxylated chitosan hydrogel (CCH) film, carboxylated chitosan power (1.0 g) was dissolved in deionized water (10 ml) at room temperature under magnetic stirring to produce carboxylated chitosan casting solution. The solution was made to stand for a while to remove air bubbles and then coat casting to the glass plate was done. Spin coating was used to prepare the casting solution as film and the film thickness was managed by spin coating at a speed of 500 rpm/min for 6 seconds. Finally, the glass plate with the solution was cross-linked through immersion in hydrochloric acid solution for 6 hours, and the resulting thickness of the CCH film was 0.532 mm. The flexible and transparent CCH film possessed several advantages such as high ionic conductivity, high electrolyte absorption capacity and high flexibility. The engendered carboxylated chitosan hydrogel film with tremendous flexibility reflects a high electrolyte uptake rate of 742.0 wt%, and a highest ionic conductivity value of 8.69×10^{-2} Scm^{-1}. All-solid-state electronic double layer capacitor (EDLC) was fabricated with carboxylated chitosan film as the gel polymer electrolyte, activated carbon film as the electrodes, and carbon cloth as collectors. The device showed a high electrochemical performance and a high specific capacitance of 45.9 Fg^{-1} at 0.5 A g^{-1}. The maximum energy density of the fabricated EDLC attained 5.2 Wh kg^{-1} at a power density of 226.6 Wkg^{-1} and a high power density of 2206.5 Wkg^{-1} at 1.9 Wh kg^{-1} within 0–0.9 V potential window [83].

Shengmei Chen et al. [84] reported for the first time, a high performance flexible solid-state zinc ion hybrid supercapacitor (ZHS) based on co-polymer derived hollow carbon spheres (HCS) as the cathode material, polyacrylamide (PAM) hydrogel as polymer electrolyte and deposited-Zn on carbon cloth as the anode material. For the preparation of the polyacrylamide (PAM) hydrogel electrolyte, an in-situ polymerization method was used. Typically, 80 mM of zinc sulphate ($ZnSO_4$) was dissolved in 40 mL of deionized (DI) water under vigorous stirring. Then, 1.0 g of acrylamide was added in the above solution under vigorously magnetic stirring at 40 ^{o}C. Next up, 2 mg of N, N'- methylenebisacrylamide as cross-linkers and 50 mg of potassium persulfate as initiator were added into the above solution and maintained at 40 ^{o}C for 2 hours. The mixture solution degassed and sealed under nitrogen atmosphere for 30 min to eliminate the dissolved oxygen. Finally, the $ZnSO_4$ PAM film obtained after a free-radical polymerization at 70 ^{o}C for 2 hours. A flexible solid-state ZHS supplies a maximum discharge capacity of 86.8 mAh g^{-1} with a maximum energy density of 59.7 Wh kg^{-1}. It also displays an excellent cycling stability with 98% capacity retention over 15,000 cycles at a current density of 1.0 Ag^{-1}. As a result of the flexible electrodes and electrolyte, the solid-state ZHS is adjustable enough to endure varying deformations such as squeezing, twisting and folding [84].

An ultra-stretchable and superior healable supercapacitors based on a double cross-linked hydrogel electrolyte was developed by Huili L. et al. [85]. They reported a nanocomposite hydrogel of a copolymer poly(2-acrylamido-2-methylpropane sulfonic acid-co-N,N-dimethylacrylamide) (poly(AMPS-co-DMAAm)) cross-linked by double linkers of Laponite (synthetic hectorite-type clay) and graphene oxide (GO). For the preparation of the poly(AMPS-co-DMAAm)/Laponite/GO nanocomposite hydrogels, an in-situ co-polymerization of the monomers AMPS and DMAAm in the presence of GO and Laponite dispersion was carried out. GO (0.32 g, 2.5 wt%) was dispersed in deionized water (7.8 mL) with continuous stirring for 20 min to obtain a homogeneous dispersion. An ultrasonic vibration for 30 min then followed this. Then, Laponite (0.16 g) was added into the GO suspension and the resulting mixture was stirred for a period of 15 min. The AMPS (0.38 g), DMAAm (1.05 mL), and initiator potassium persulfate (KPS; 0.01 g) were added with stirring for 15 min as one of them was added. Finally, to obtain the

precursor, catalyst of N,N,N',N'-tetramethylethylenediamine (TEMED; 10 µL) was blended along with stirring for 5 min. The precursor was transferred into a homemade mold, and followed by an in-situ free radical co-polymerization in ambient temperature for a period of 24 h. The as-prepared hydrogel films (thickness spanning from 0.8 to 1.5 mm) were cut into desired shapes for characterization or use in supercapacitors. The resultant hydrogel exhibits high mechanical stretchability (tensile strength of 34 KPa and stretchability of 1173%), excellent ionic conductivity, and superior healable performance. Supercapacitors made by utilizing this hydrogel as a gel electrolyte not just only display an ultrahigh mechanical stretchability of 1000%, but also they attain repeated healable performance under infrared light irradiation and upon heating. More significantly, the broken/healed supercapacitor also possesses an ultrahigh stretchability up to 900% with only a slight performance decrease of 15%. This vaunted hydrogel electrolyte could be easily functionalized by integrating other functional components, and also they can be extended for use in other portable and wearable energy related devices with multifunction [85].

A highly adhesive poly(ionic liquid) and a commercial ionic liquid (PIL/IL) gel polymer electrolyte for use in flexible solid state SCs was prepared by Sandra A. Alexandre et. al. [86]. In their work, they demonstrated the preparatio of a novel gel polymer electrolyte (GPE) with significant adhesive characteristics by amalgamating a synthesized poly(ionic liquid) which consists of poly(1-vinyl-3-propylimidazolium bis(fluorosulfonyl)imide) (poly(VPIFSI)) and a commercial ionic liquid, 1-ethyl-3-methylimidazolium bis(fluorosulfonyl)imide (EMIFSI). The polymeric ionic liquid, poly(1-vinyl-3-propylimidazolium bis(fluorosulfonyl)imide) poly(VPIFSI) was synthesized in two stages. Firstly, the direct polymerization of the IL monomer VPIBr occurred to produce the poly(ionic liquid) 1-vinyl-3-propylimidazoliumbromide-poly(VPIBr). The second stage deals with the modification of the synthesized poly(ionic liquid) by means of a simple ion exchange reaction between the poly(VPIBr) and the lithium bis(fluorosulfonyl)imide (LiFSI) to produce the poly(PVIFSI). The PIL/IL-GPE containing the poly(VPIFSI) as the host polymer was prepared by the solution casting method in proportions of 30, 50 and 70 wt% of IL. 0.5 g of poly(VPIFSI) was separately and completely dissolved in 5 mL of acetone for 8 h. EMIFSI ionic liquid was then added to the solution in corresponding quantities and mixed until a homogeneous solution was attained.

The effect of the PIL/IL-GPE (50 wt.% of IL) on the properties of a flexible solid state SC was investigated with the aid of electrochemical impedance spectroscopy (EIS), cyclic voltammetry (CV) and the galvanostatic charge/discharge technique that allows synchronous measurements or determination of the cell voltage and the potential of the positive and negative electrodes. The properties of the adhesive PIL/IL-GPE, include high conductivity, good interaction between the PIL matrix and the IL liquid phase that hinders leakage to ensure safety, good adherability and wettability of the gel electrolyte on the electrode surface etc. All these excellent properties have been utilized to produce a device with an improved rate capability and cyclability that hardly experiences any changes in specific capacitance, energy density and power density of the cell when folded [86].

Pankaj Tuhania et. al. [87] developed a novel ionic liquid (IL)-doped solid polymer electrolyte based on poly (vinylidene fluoride-co-hexafluoropropylene) as host polymer (PVDF-HFP) and low-viscosity 1-ethyl-3-methylimidazolium thiocyanate as dopant for efficient electrochemical double-layer capacitors (EDLC). Pure and IL-doped electrolyte films were prepared through the process of solution casting. PVDF-HFP dissolved in acetone using magnetic stirrer for 2 h and a directly chosen amount of IL was added to maintain its desired ratio (by wt.) in PVDF-HFP films to prepare IL-doped films. To make a homogenous viscous solution of polymer-IL, the mixture was kept on magnetic stirrer overnight. The prepared solution was kept for drying in polypropylene petri dishes at room temperature, this was then preceded by vacuum drying to eliminate the remaining traces of acetone (if any) to achieve freestanding films of pure PVDF-HFP and IL-doped films. The characterization of the films was done using conductivity measurements; electrochemical stability window (ESW) measurements, optical microscopy, and Fourier transform infrared (FTIR) spectroscopy. Finally, they prepared a device using the maximum conductivity IL-doped film as electrolyte material. Electrochemical impedance spectroscopy of the ionic liquid doped polymer electrolyte revealed a six orders of magnitude enhancement in conductivity behavior of the electrolyte films by IL doping. A linear sweep voltammetric investigation and study of the electrolyte films revealed a robust electrochemical stability window of 3.6 V. Polarized optical microscopy of the synthesized films showed a reduction in the degree of crystallinity brought about by IL doping. The FTIR spectroscopy measurement further affirms

the composite nature of the film. For an 80% of the ionic-doped system, the maximum conductivity value obtained is 2.65 mS/cm. Furthermore, the developed EDLC shows a specific capacitance value of 2.36 Fg^{-1} [87].

REFERENCES

[1] M. Winter and R. J. Brodd, "What are batteries, fuel cells, and supercapacitors?," *Chem. Rev.*, vol. 104, no. 10, pp. 4245–69, 2004.

[2] I. Climate, "World energy consumption (Quadrilion Btu) Year."

[3] F. Béguin, V. Presser, A. Balducci, and E. Frackowiak, "Carbons and Electrolytes for Advanced Supercapacitors," *Adv. Mater.*, vol. 26, no. 14, pp. 2219–2251, Apr. 2014.

[4] Marin S. Halper James C. Ellenbogen, "Supercapacitors: A Brief Overview," *Biosens. Bioelectron.*, vol. 25, no. 7, pp. 1629–1634, 2010.

[5] R. Zhang, "a Study of Flexible Supercapacitors: Design, Manufacture and Testing," no. June, 2016.

[6] R. Kotz and M. Carlen, "Principles and applications of Caps," vol. 45, pp. 1–16, 2000.

[7] J. R. Miller and P. Simon, "Materials science: Electrochemical capacitors for energy management," *Science*, vol. 321, no. 5889, pp. 651–652, 2008.

[8] S. M. Chen, R. Ramachandran, V. Mani, and R. Saraswathi, "Recent advancements in electrode materials for the high-performance electrochemical supercapacitors: A review," *Int. J. Electrochem. Sci.*, vol. 9, no. 8, pp. 4072–4085, 2014.

[9] M. D. Stoller and R. S. Ruoff, "Best practice methods for determining an electrode material's performance for ultracapacitors," *Energy Environ. Sci.*, vol. 3, no. 9, pp. 1294–1301, 2010.

[10] B. E. Conway and W. G. Pell, "Double-layer and pseudocapacitance types of electrochemical capacitors and their applications to the development of hybrid devices," *J. Solid State Electrochem.*, vol. 7, no. 9, pp. 637–644, 2003.

[11] N. Elgrishi, K. J. Rountree, B. D. McCarthy, E. S. Rountree, T. T. Eisenhart, and J. L. Dempsey,

"A Practical Beginner's Guide to Cyclic Voltammetry," *J. Chem. Educ.*, vol. 95, no. 2, pp. 197–206, 2018.

[12] M. Khawaja, "Synthesis and Fabrication of Graphene/ Conducting Polymer/ Metal Oxide Nanocomposite Materials for Supercapacitor Applications," no. January, 2015.

[13] S. Zhang and N. Pan, "Supercapacitors performance evaluation," *Adv. Energy Mater.*, vol. 5, no. 6, pp. 1–19, 2015.

[14] G. Wang, L. Zhang, and J. Zhang, "A review of electrode materials for electrochemical supercapacitors," *Chem. Soc. Rev.*, vol. 41, no. 2, pp. 797–828, 2012.

[15] Y. Xie, X. Sheng, D. Xie, Z. Liu, X. Zhang, and L. Zhong, "Fabricating graphene hydrogels with controllable pore structure via one-step chemical reduction process," *Carbon N. Y.*, vol. 109, pp. 673–680, 2016.

[16] P.-O. Logerais, O. Riou, M. A. Camara, and J.-F. Durastanti, "Study of Photovoltaic Energy Storage by Supercapacitors through Both Experimental and Modelling Approaches," *J. Sol. Energy*, vol. 2013, pp. 1–9, 2013.

[17] G. A. M Ali, M. M. Yusoff, and K. Feng Chong, "Graphene : Electrochemical Production And Its Energy Storage Properties," vol. 11, no. 16, 2016.

[18] Z. S. Iro, C. Subramani, and H. Y. Hafeez, "Study of Asymmetric Hybrid Supercapacitor using Carbon and Metal Oxides as Electrode Materials," *Indian J. Sci. Technol.*, vol. 9, no. 29, Aug. 2016.

[19] S. Kannappan, A. S. Pandian, W. Lu, J.-H. Jang, H. Yang, and Y. S. Lee, "Graphene supercapacitor with both high power and energy density," *Nanotechnology*, vol. 28, no. 44, p. 445401, 2017.

[20] A. A. F. Lufrano, P. Staiti, E.J. Juarez-Perez, J.A. Menendez *et al.*, "Carbon xerogel and manganese oxide capacitive materials for advanced supercapacitors," *Int. J. Electrochem.*

Sci., vol. 6, no. 3, pp. 596–612, 2011.

[21] K. Lota, A. Sierczynska, I. Acznik, and G. Lota, "Effect of aqueous electrolytes on electrochemical capacitor capacitance," *Chemik*, vol. 67, no. 11, pp. 1138–1145, 2013.

[22] A. G. Pandolfo and A. F. Hollenkamp, "Carbon properties and their role in supercapacitors," *J. Power Sources*, vol. 157, no. 1, pp. 11–27, 2006.

[23] N. Syarif, T. A. Ivandini, and W. Wibowoa, "Direct Synthesis Carbon/Metal Oxide Composites for Electrochemical Capacitors Electrode," *Int. Trans. J. Eng. Manag. Appl. Sci. Technol.*, vol. 3, no. 1, pp. 21–34, 2012.

[24] J. Li, X. Cheng, A. Shashurin, and M. Keidar, "Review of Electrochemical Capacitors Based on Carbon Nanotubes and Graphene," *Graphene*, vol. 01, no. 01, pp. 1–13, 2012.

[25] C. Du and N. Pan, "Carbon Nanotube-Bases Supercapacitors," *Nanotechnol. Law Bus.*, pp. 569–576, 2007.

[26] Q. Cheng, J. Tang, J. Ma, H. Zhang, N. Shinya, and L. C. Qin, "Graphene and carbon nanotube composite electrodes for supercapacitors with ultra-high energy density," *Phys. Chem. Chem. Phys.*, vol. 13, no. 39, pp. 17615–17624, 2011.

[27] W. D. Callister and D. G. Rethwisch, "Materials Science and Engineering 9th Edition," *Comput. Sci. Eng.*, 2014.

[28] T. K. Enock, C. K. King'ondu, A. Pogrebnoi, and Y. A. C. Jande, "Status of Biomass Derived Carbon Materials for Supercapacitor Application," *Int. J. Electrochem.*, vol. 2017, pp. 1–14, 2017.

[29] H. Wang, Q. Hao, X. Yang, L. Lu, and X. Wang, "Graphene oxide doped polyaniline for supercapacitors," *Electrochem. commun.*, vol. 11, no. 6, pp. 1158–1161, 2009.

[30] T. Kuilla, S. Bhadra, D. Yao, N. H. Kim, S. Bose, and J. H. Lee, "Recent advances in graphene based polymer composites," *Prog. Polym. Sci.*, vol. 35, no. 11, pp. 1350–1375, 2010.

[31] W. Zhou *et al.*, "Fabrication of Co_3O_4-reduced graphene oxide scrolls for high-performance supercapacitor electrodes," *Phys. Chem. Chem. Phys.*, vol. 13, no. 32, pp. 14462–14465, 2011.

[32] C. Liu, Z. Yu, D. Neff, A. Zhamu, and B. Z. Jang, "Graphene-based supercapacitor with an ultrahigh energy density," *Nano Lett.*, vol. 10, no. 12, pp. 4863–4868, 2010.

[33] D. C. Marcano *et al.*, "Correction to Improved Synthesis of Graphene Oxide," *ACS Nano*, vol. 12, no. 2, pp. 2078–2078, 2018.

[34] D. W. Wang *et al.*, "Fabrication of Graphene / Polyaniline," *ACS Nano*, vol. 3, no. 7, pp. 1745–1752, 2009.

[35] L. Sui *et al.*, "Supercapacitive behavior of an asymmetric supercapacitor based on a Ni(OH)2/XC-72 composite," *New J. Chem.*, vol. 39, no. 12, pp. 9363–9371, 2015.

[36] P. He, K. Yang, W. Wang, F. Dong, L. Du, and Y. Deng, "Reduced graphene oxide-$CoFe_2O_4$ composites for supercapacitor electrode," *Russ. J. Electrochem.*, vol. 49, no. 4, pp. 359–364, 2013.

[37] S. F. Besharat, M. Manteghian, and M. Abdollahi, "Study of Polypyrrole/Graphene Oxide Nanocomposite Structural and Morphological Changes Including Porosity," *Polym. Sci. Ser. B*, vol. 60, no. 5, pp. 664–674, 2018.

[38] A. Moftah and A. Al Shetiti, "Fig.2 Supercapacitor cell Fig.3 Electric double-layer capacitor," vol. 3, no. 3, 2015.

[39] S. Chen, J. Zhu, X. Wu, Q. Han, and X. Wang, "2010Graphene oxide-Mno_2," *ACS Nano*, vol. 4, no. 5, pp. 2822–2830, 2010.

[40] I. Acznik, K. Lota, A. Sierczynska, and G. Lota, "Carbon-supported manganese dioxide as electrode material for asymmetric electrochemical capacitors," *Int. J. Electrochem. Sci.*, vol. 9, no. 5, pp. 2518–2534, 2014.

[41] H. C. Chen *et al.*, "A novel randomly textured phosphor structure for highly efficient white light-emitting diodes," *Nanoscale Res. Lett.*, vol. 7, pp. 1–5, 2012.

[42] H. Y. Wu and H. W. Wang, "Electrochemical synthesis of nickel oxide nanoparticulate films on nickel foils for high-performance electrode materials of supercapacitors," *Int. J. Electrochem. Sci.*, vol. 7, no. 5, pp. 4405–4417, 2012.

[43] T. P. Gujar, W. Y. Kim, I. Puspitasari, K. D. Jung, and O. S. Joo, "Electrochemically deposited nanograin ruthenium oxide as a pseudocapacitive electrode," *Int. J. Electrochem. Sci.*, vol. 2, no. 9, pp. 666–673, 2007.

[44] H. X. Wang, W. Zhang, H. Chen, and W. T. Zheng, "Towards unlocking high-performance of supercapacitors: From layered transition-metal hydroxide electrode to redox electrolyte," *Sci. China Technol. Sci.*, vol. 58, no. 11, pp. 1779–1798, 2015.

[45] L. Cao, F. Xu, Y. Y. Liang, and H. L. Li, "Preparation of the novel nanocomposite Co(OH)2/ultra-stable Y zeolite and its application as a supercapacitor with high energy density," *Adv. Mater.*, vol. 16, no. 20, pp. 1853–1857, 2004.

[46] V. Augustyn, P. Simon, and B. Dunn, "Pseudocapacitive oxide materials for high-rate electrochemical energy storage," *Energy Environ. Sci.*, vol. 7, no. 5, pp. 1597–1614, 2014.

[47] V. A. Online, R. Luque, R. V Hadi, H. Salehzadeh, V. Moradi, and A. R. Solymani, "RSC Advances."

[48] C. Zhong, Y. Deng, W. Hu, J. Qiao, L. Zhang, and J. Zhang, "A review of electrolyte materials and compositions for electrochemical supercapacitors," *Chem. Soc. Rev.*, vol. 44, no. 21, pp. 7484–7539, 2015.

[49] F. Soavi *et al.*, "Miniaturized supercapacitors: key materials and structures towards autonomous and sustainable devices and systems," *J. Power Sources*, vol. 326, pp. 717–725, 2016.

[50] T. N. Y. Khawula, K. Raju, P. J. Franklyn, I. Sigalas, and K. I. Ozoemena, "Symmetric pseudocapacitors based on molybdenum disulfide (MoS_2)-modified carbon nanospheres: Correlating physicochemistry and synergistic interaction on energy storage," *J. Mater. Chem. A*, vol. 4, no. 17, pp. 6411–6425, 2016.

[51] N. Li, S. Tang, and X. Meng, "Preparation of Pt-GO composites with high-number-density Pt nanoparticles dispersed uniformly on GO nanosheets," *Prog. Nat. Sci. Mater. Int.*, vol. 26, no. 2, pp. 139–144, 2016.

[52] Y. Chen, X. Zhang, H. Zhang, X. Sun, D. Zhang, and Y. Ma, "High-performance supercapacitors based on a graphene-activated carbon composite prepared by chemical activation," *RSC Adv.*, vol. 2, no. 20, pp. 7747–7753, 2012.

[53] M. Vangari, T. Pryor, and L. Jiang, "Supercapacitors: Review of Materials and Fabrication Methods," *J. Energy Eng.*, vol. 139, no. 2, pp. 72–79, 2012.

[54] C. Zhong, Y. Deng, W. Hu, J. Qiao, L. Zhang, and J. Zhang, "A review of electrolyte materials and compositions for electrochemical supercapacitors," *Chem. Soc. Rev.*, vol. 44, no. 21, pp. 7484–7539, 2015.

[55] M. D. Stoller *et al.*, "Activated graphene as a cathode material for Li-ion hybrid supercapacitors," *Phys. Chem. Chem. Phys.*, vol. 14, no. 10, pp. 3388–3391, 2012.

[56] "Oka for Chiamaka Cynthia Supervised by Professor E. Ntsoenzok African University of Science and Technology," no. June, 2016.

[57] X. Zang, C. Shen, M. Sanghadasa, and L. Lin, "High-Voltage Supercapacitors Based on Aqueous Electrolytes," *ChemElectroChem*, vol. 6, no. 4, pp. 976–988, 2019.

[58] S. Shivakumara, B. Kishore, T. R. Penki, and N. Munichandraiah, "Symmetric supercapacitor based on partially exfoliated and reduced graphite oxide in neutral aqueous electrolyte," *Solid State Commun.*, vol. 199, pp. 26–32, 2014.

[59] K. Fic, M. Meller, and E. Frackowiak, "Interfacial Redox Phenomena for Enhanced Aqueous Supercapacitors," *J. Electrochem. Soc.*, vol. 162, no. 5, pp. A5140–A5147, 2015.

[60] C. Zhao and W. Zheng, "A Review for Aqueous Electrochemical Supercapacitors," *Front. Energy Res.*, vol. 3, no. May, pp. 1–11, 2015.

[61] J. Menzel, K. Fic, and E. Frackowiak, "Hybrid aqueous capacitors with improved energy/power performance," *Prog. Nat. Sci. Mater. Int.*, vol. 25, no. 6, pp. 642–649, 2015.

[62] A. Yu, V. Chabot, and J. Zhang, *Electrochemical Supercapacitors for Energy Storage and Delivery*. 2018.

[63] S. P. Ong, O. Andreussi, Y. Wu, N. Marzari, and G. Ceder, "Chem. Mater." pp. 902035–902035, 2009.

[64] E. Lim *et al.*, "Advanced Hybrid Supercapacitor Based on a Mesoporous Niobium," *ACS Nano*, vol. 8, no. 9, pp. 8968–8978, 2014.

[65] N. Ashok Kumar and J. B. Baek, "Electrochemical supercapacitors from conducting polyaniline-graphene platforms," *Chem. Commun.*, vol. 50, no. 48, pp. 6298–6308, 2014.

[66] S. Dutta and S. De, "Few layered vanadyl phosphate nano sheets-MWCNT hybrid as an electrode material for supercapacitor application," *AIP Conf. Proc.*, vol. 1728, 2016.

[67] K. Gupta *et al.*, "High surface area carbon from polyacrylonitrile for high-performance electrochemical capacitive energy storage," *J. Mater. Chem. A*, vol. 4, no. 47, pp. 18294–18299, 2016.

[68] C. M. Yang *et al.*, "Nanowindow-regulated specific capacitance of supercapacitor electrodes of single-wall carbon nanohorns," *J. Am. Chem. Soc.*, vol. 129, no. 1, pp. 20–21, 2007.

[69] A. Linares-Solano, M. A. Á. Lillo-Ródenas, J. P. Marco-Lozar, M. Kunowsky, and A. J. J. Romero-Anaya, "NaOH and KOH for preparing activated carbons used in energy and

environmental applications," *Int. J. Energy, Environ. Econ.*, vol. 20, no. 4, pp. 355–387, 2012.

[70] G. Camino, "Guest editorial," *Polym. Degrad. Stab.*, vol. 77, no. 2, p. 185, 2002.

[71] A. Lewandowski and M. Galinski, "Practical and theoretical limits for electrochemical double-layer capacitors," *J. Power Sources*, vol. 173, no. 2 SPEC. ISS., pp. 822–828, 2007.

[72] M. Bier *et al.*, *Small-Angle X-ray Scattering Study of Au Nanoparticles Dispersed in the Ionic Liquids 1-Alkyl-3-methylimidazolium Tetrafluoroborate*, vol. 8, no. 1. 2011.

[73] M. Armand, F. Endres, D. R. MacFarlane, H. Ohno, and B. Scrosati, "Ionic-liquid materials for the electrochemical challenges of the future," *Nat. Mater.*, vol. 8, no. 8, pp. 621–629, 2009.

[74] A. Eftekhari, "Supercapacitors utilising ionic liquids," *Energy Storage Mater.*, vol. 9, no. September, pp. 47–69, 2017.

[75] S. Fleischmann *et al.*, "High voltage asymmetric hybrid supercapacitors using lithium- and sodium-containing ionic liquids," *Energy Storage Mater.*, vol. 16, no. June 2018, pp. 391–399, 2019.

[76] A. Brandt, S. Pohlmann, A. Varzi, A. Balducci, and S. Passerini, "Ionic liquids in supercapacitors," *MRS Bull.*, vol. 38, no. 7, pp. 554–559, 2013.

[77] X. Hu, Y. Chen, Z. Hu, Y. Li, and Z. Ling, "All-Solid-State Supercapacitors Based on a Carbon-Filled Porous/Dense/Porous Layered Ceramic Electrolyte," *J. Electrochem. Soc.*, vol. 165, no. 7, pp. A1269–A1274, 2018.

[78] L. Wu *et al.*, "Flexible solid-state symmetric supercapacitors based on MnO_2 nanofilms with high rate capability and long cyclability," *AIP Adv.*, vol. 3, no. 8, pp. 2–7, 2013.

[79] Z. Niu *et al.*, "Highly stretchable, integrated supercapacitors based on single-walled carbon nanotube films with continuous reticulate architecture," *Adv. Mater.*, vol. 25, no. 7, pp.

1058–1064, 2013.

[80] D. P. Dubal, N. R. Chodankar, D. H. Kim, and P. Gomez-Romero, “Towards flexible solid-state supercapacitors for smart and wearable electronics,” *Chem. Soc. Rev.*, vol. 47, no. 6, pp. 2065–2129, 2018.

[81] Y. J. Kang, Y. Yoo, and W. Kim, “3-V Solid-State Flexible Supercapacitors with Ionic-Liquid-Based Polymer Gel Electrolyte for AC Line Filtering,” *ACS Appl. Mater. Interfaces*, vol. 8, no. 22, pp. 13909–13917, 2016.

[82] H. T. Jeong, J. F. Du, and Y. R. Kim, “Development of Flexible Energy Storage Device by Using Polymer Electrolyte Based on Ionic Liquid,” *ChemistrySelect*, vol. 2, no. 21, pp. 6057–6061, 2017.

[83] H. Yang, Y. Liu, L. Kong, L. Kang, and F. Ran, “Biopolymer-based carboxylated chitosan hydrogel film crosslinked by HCl as gel polymer electrolyte for all-solid-sate supercapacitors,” *J. Power Sources*, vol. 426, no. March, pp. 47–54, 2019.

[84] S. Chen, L. Ma, K. Zhang, M. Kamruzzaman, C. Zhi, and J. A. Zapien, “A flexible solid-state zinc ion hybrid supercapacitor based on co-polymer derived hollow carbon spheres,” *J. Mater. Chem. A*, vol. 7, no. 13, pp. 7784–7790, 2019.

[85] H. Li *et al.*, “Ultra stretchable and superior healable supercapacitors based on a double cross-linked hydrogel electrolyte,” *Nat. Commun.*, vol. 10, no. 1, pp. 1–8, 2019.

[86] S. A. Alexandre, G. G. Silva, R. Santamaría, J. P. C. Trigueiro, and R. L. Lavall, “A highly adhesive PIL/IL gel polymer electrolyte for use in flexible solid state supercapacitors,” *Electrochim. Acta*, vol. 299, pp. 789–799, 2019.

[87] P. Tuhania *et al.*, “PVDF-HFP and 1-ethyl-3-methylimidazolium thiocyanate–doped polymer electrolyte for efficient supercapacitors,” *High Perform. Polym.*, vol. 30, no. 8, pp. 911–917, 2018.

CHAPTER THREE

EXPERIMENTAL PROCEDURE AND CHARACTERIZATION TECHNIQUES

3.1 Production of the various polymer electrolyte and electrode material

3.1.1 Materials

Polyethylene oxide (PEO, Sigma–Aldrich, mol. Wt. = 600,000), Lithium perchlorate ($LiClO_4$, Sigma–Aldrich) and ionic liquid (IL), tetraethylammonium tetrafluoroborate ($TEABF_4$), Purity >98%, were obtained from Sigma–Aldrich, Germany. Synthetic graphite (Merck powder, <20 µm), chitosan, acetic acid, conducting carbon was also used. Methanol was the sole solvent throughout the course of this experimental work.

3.1.2 Preparation of Polymer Electrolyte Films

Polymer electrolyte films of seven (7) different compositions were prepared. The samples were denoted as sample 1, 2, 3a, 3b, 3c, 3d and 3e. The composition of the different electrolytes are as follows: pristine PEO which corresponds to 1, PEO:10 wt. % IL corresponds to 2, and (PEO:10 wt. % $LiClO_4$) + x wt. % IL (x = 0 (corresponds to 3a), 5 (corresponds to 3b), 10 (corresponds to 3c), 15 (corresponds to 3d), 20 (corresponds to 3e)), were prepared by the orthodox solution casting technique. The films could be obtained as ''freestanding films'' for application as solid polymer electrolytes. The PEO, $LiClO_4$ and IL, in desired ratios, were mixed with methanol and stirred vigorously for one hour. The resultant homogeneous solution was placed in a polypropylene petri dish and the solvent was allowed to evaporate slowly in ambient condition. After complete evaporation of the solvent, free standing films of different compositions were obtained [1].

3.1.3 Preparation of the electrode material

Acetic acid solution was prepared in a concentration of 3 wt. % of acetic acid in water inside a 50 ml beaker. The mixture was stirred for 10 minutes at 300 rpm. The homogenously stirred solutions

were then used in the preparation of the chitosan-based binders of wt. concentration of 1.2 %. This was allowed to stir until all chitosan dissolved giving a homogeneous and clear viscous solution. The as-prepared chitosan binders were then used to prepare the electrode pastes in the weight percent ratio of 85:10:5 in terms of graphite (active carbon), binder and conducting carbon; in a beaker and then allowed to stir to homogeneity [2].

The prepared pastes were coated on a carbon cloth substrate, which have been previously weighed. The coated substrates were then oven-dried for 12 h at 40 ^{0}C to ensure that the electrodes were completely dried. The mass of the dried coated substrates were taken and the difference between dried coated substrates and uncoated substrates were recorded [3]. For the full device, fabrication pairs of circular cut coated carbon cloth substrates with equal masses were used to fabricate a coin cell device using the novel as prepared gel polymer electrolyte prepared as mentioned above. Filter papers were used as separators for the device.

3.2 Materials Characterization

3.2.1 Fourier Transform Infra-red Resonance (FTIR) Spectroscopy of Electrolyte Samples

Fourier transform infrared spectroscopy was carried out on the gel polymer electrolyte samples using a Thermo Scientific Nicolet iS5 spectrometer within a wavenumber range of 500 – 4000 cm^{-1}.

3.3 Electrochemical Analysis

3.3.1 Cyclic Voltammetry (CV)

The CV measurement were carried out in a two-electrode configuration for each cell. The 2-electrode CV was conducted using the fabricated symmetrical devices, with a Gamry reference 600 workstation supplying the required potential. This test was carried out at scan rates of 5 mV s^{-1} to 100 mV s^{-1} and voltage varied from of 0.6 V to 2.3 V; depending on the electrolyte used to fabricate the device. The CV test was carried out in 2 parts: varying voltage at constant scan rate and varying scan rate at constant voltage. The specific capacitance for the 2-electrode experiment was obtained by [3]:

$$C_{sp} = \frac{4Charge}{m\,V} \quad \ldots \quad \ldots \quad \ldots \quad \ldots \quad \textbf{(3.1)}$$

Where; C_{sp} is the Specific Capacitance (F g^{-1}), the charge corresponds to the area of voltagramm (C), m is the Active Mass (g), V represents the potential window (V). Also, the energy – density was obtained by [4]:

$$E_D = \frac{0.5\,Charge\,V^2}{3.6\,m} \quad \ldots \quad \ldots \quad \ldots \quad \ldots \quad \textbf{(3.2)}$$

where; E_D is the energy Density (kW hg^{-1}), as usual, the charge corresponds to the area of voltagramm (C), m is the Active Mass (g), V represents the potential window (V), While power – density was obtained by [4]:

$$P_D = \frac{4\,V^2}{m\,R} \quad \ldots \quad \ldots \quad \ldots \quad \ldots \quad \textbf{(3.3)}$$

Where; P_D is the power density (kW g^{-1}), V is the potential window (V), m is the active mass (g), and R is the equivalent series resistance.

3.3.2 Electrochemical Impedance Spectroscopy

The ion kinetics within the electrodes was probed using the electrochemical impedance spectroscopy (EIS) with an amplitude of 10 mV at the frequency range of 10 mHz to 100 kHz [4]. A Bode plot which the relationship between the phase angle and the frequency was obtained alongside a Nyquist which showed the relationship between the imaginary and real part of the impedance of electrode material, equivalent series resistance of device and the charge transfer resistance [5].

REFERENCES

[1] S. K. Chaurasia, R. K. Singh, and S. Chandra, "Dielectric relaxation and conductivity studies on (PEO:$LiClO_4$) polymer electrolyte with added ionic liquid [BMIM][PF_6]: Evidence of ion-ion interaction," *J. Polym. Sci. Part B Polym. Phys.*, vol. 49, no. 4, pp. 291–300, 2011.

[2] V. Subramanian, C. Luo, A. M. Stephan, K. S. Nahm, S. Thomas, and B. Wei, "Supercapacitors from activated carbon derived from banana fibers," *J. Phys. Chem. C*, vol. 111, no. 20, pp. 7527–7531, 2007.

[3] F. O. Ochai-Ejeh *et al.*, "High electrochemical performance of hierarchical porous activated carbon derived from lightweight cork (Quercus suber)," *J. Mater. Sci.*, vol. 52, no. 17, pp. 10600–10613, 2017.

[4] P. Cheng *et al.*, "Hierarchically porous carbon by activation of shiitake mushroom for capacitive energy storage," *Carbon*, vol. 93, no. July 2016, pp. 315–324, 2015.

[5] G. Wang, L. Zhang, and J. Zhang, "A review of electrode materials for electrochemical supercapacitors," *Chem. Soc. Rev.*, vol. 41, no. 2, pp. 797–828, 2012.

CHAPTER FOUR

RESULTS AND DISCUSSIONS

4.1 Fourier Transform Infra-red Resonance Analysis of Electrolytes

The pristine polymer PEO is has a very low conductivity. However, the C-O-C ether group of PEO can form a complex with the cations of many ionic salts, which leads to the increase in its ionic conductivity. The complexation of the salt cation (say Li^+) and IL-Ca tion (TEA^+) in PEO, apart from introducing conducting ions also change the degree of crystallinity, which is an additional help for cation/anion mobility [1], [2], [3]. A more direct proof that ether oxygen of C-O-C bond of PEO is involved in the complexation comes from the Fourier transform infrared resonance (FTIR) results. The Figure 4.1 shows the vibrational spectra of the seven (7) polymer electrolyte samples.

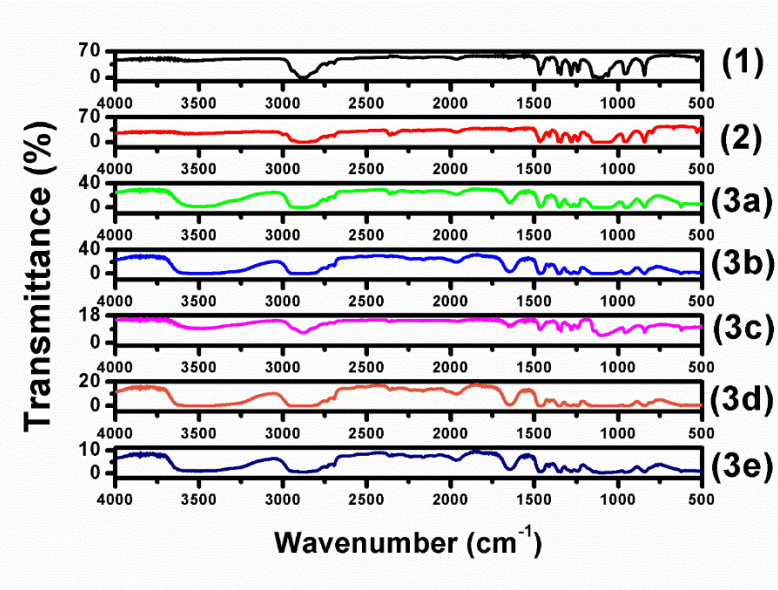

Figure 4. 1: FTIR spectra of the 7 electrolyte samples labelled 1, 2, 3a, 3b, 3c, 3d and 3e

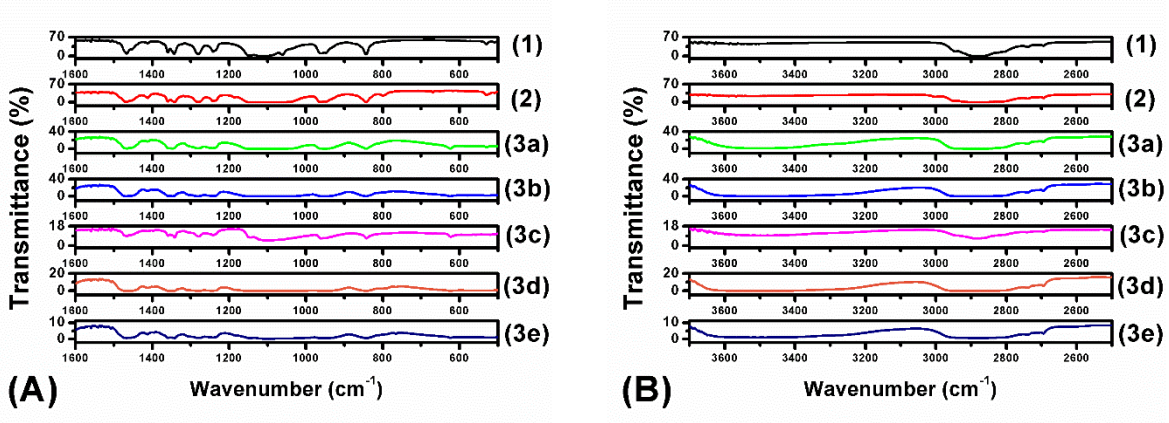

Figure 4. 2: Expanded spectra of (A) C-O-C vibration of PEO and (B) C-H and O-H/N-H stretching of IL for *the 7 electrolyte samples labelled 1, 2, 3a, 3b, 3c, 3d and 3e*

The C-O-C stretching vibrations of PEO which are observed at approximately 1000–1 200 cm^{-1} are particularly interesting for our study because the cations of the salt as well as IL added to PEO are more likely to complex with ether oxygen of this C-O-C bond [4], [5]. The C-O-C vibrations of PEO have three peaks viz. peak A at 1060.66 cm^{-1}, a broad peak B centered at 1113.69 cm^{-1} and peak C appearing at 1114.88 cm^{-1}. The expanded FTIR for these relevant vibrations are shown in Figure 4.2 and respective peak positions are given in Table 4.1 from which the following inferences can be drawn

- The peaks related to C-O-C vibrations of pristine PEO at 1060.66 cm^{-1}, 1113.69 cm^{-1} and 1114.88 cm^{-1} shift to 1024.98, 1087.17, and 1148.80 cm^{-1}, respectively on addition of salt $LiClO_4$. This indicates that Li^+ cation is complexing with ether oxygen C-O-C of PEO.
- The C-O-C peaks of pristine PEO occurring at 1060.66, 1113.69, and 1114.88 cm^{-1} also shift on addition of IL only. Peak shift are observed at 1060, 1102, and 1149 cm^{-1}, respectively. This indicates that the (TEA^+) cation of IL also complexes with the C-O-C group of PEO.
- As both IL cation and Li^+ complex with PEO, it is expected that the peak positions in mixed polymer electrolyte (PEO:$LiClO_4$ + IL) will be different than pristine PEO as is given in Table 1. The peaks of C-O-C vibration of pristine PEO occurring at 1060.66, 1113.69, and 1114.88 cm^{-1} shift to 1024.98, 1095.37, and 1148.88 cm^{-1}, respectively for PEO:10 wt. % $LiClO_4$ + 5

wt. % IL system. Also the C=C group which is absent in electrolyte samples 1 and 2, becomes obvious in 3a, 3b and 3c at a wave number of 1644.98cm^{-1}.

- In view of (2) above, the vibrations of IL cation imidazolium ring will change, when complexed with ether oxygen of C-O-C group of PEO chain. The expanded FTIR spectra of C-H and O-H stretching vibration of (TEA^+) cation ring in the polymer electrolyte samples is given in Figure 4.2(B and listed in Table 1. It is clear that the C-H stretching vibrations remain somewhat constant for all electrolyte polymer samples. Worthy to note is that the O-H stretching which is absent for electrolyte samples 1 and 2 is present in 3a, 3b and 3c. It is at a constant value of 3500 cm^{-1}.

Table 4. 1: Changes in C-O-C vibrations of PEO and CH stretching vibrations of IL cation (TEA^+) ring on complexation

Peak Positions	**Pristine PEO**	**PEO + IL**	**PEO + 10 wt. % $LiClO_4$ + 0 wt. % IL**	**PEO + 10 wt. % $LiClO_4$ + 5 wt. % IL**	**PEO + 10 wt. % $LiClO_4$ + 10 wt. % IL**
PEO related C-O-C vibrations (A)	1060.66 cm^{-1}	1032.21 cm^{-1}	1024.98 cm^{-1}	1024.98 cm^{-1}	Absent
PEO related C-O-C vibrations (B)	1113.69 cm^{-1}	1095.36 cm^{-1}	1087.17 cm^{-1}	1095.37 cm^{-1}	1095.37 cm^{-1}
PEO related C-O-C vibrations (C)	1114.88 cm^{-1}	1148.88 cm^{-1}	1148.88 cm^{-1}	1148.88 cm^{-1}	1148.88 cm^{-1}
C=C	Absent	Absent	1644.98 cm^{-1}	1644.98 cm^{-1}	1644.98 cm^{-1}
C-H stretching	2884.03 cm^{-1}	2884.03 cm^{-1}	2884.03	2884.03 cm^{-1}	2874.86 cm^{-1}
O-H stretching	Absent	Absent	3500 cm^{-1}	3500 cm^{-1}	3500 cm^{-1}

4.2 Electrochemical Analysis

4.2.1 Cyclic Voltammetry and Electrochemical Impedance Spectroscopy

Figure 4.3(A) represents the CV of the supercapacitor device utilizing electrolyte sample 1 (Pure PEO). A constant scan rate at 50 mV s^{-1} and the potential varied from 0.3 V to 0.6 V at increasing interval of 0.1 V. The maximum operating voltage of the device was 0.6 V. Figure 4.3(A) shows a quasi-rectangular shape, which shows that the produced electrodes exhibit the typical EDLCs behavior. Figure 4.3(B) represents the CV of the supercapacitor device utilizing electrolyte sample 1 (Pure PEO) at a constant potential of 0.6V and varying scan rate from 5 mV s^{-1} to 100 mV s^{-1}. The scan rate of the experiment controls how fast the applied potential is scanned. Faster scan rates lead to a decrease in the size of the diffusion layer; as a consequence, higher currents are observed [6]. The CV curves with a maximum potential window of 0.6 V of the EDLC at different scan rates showed quasi-rectangular shapes, indicating low charge transfer resistance and relatively ideal capacitance characteristics.

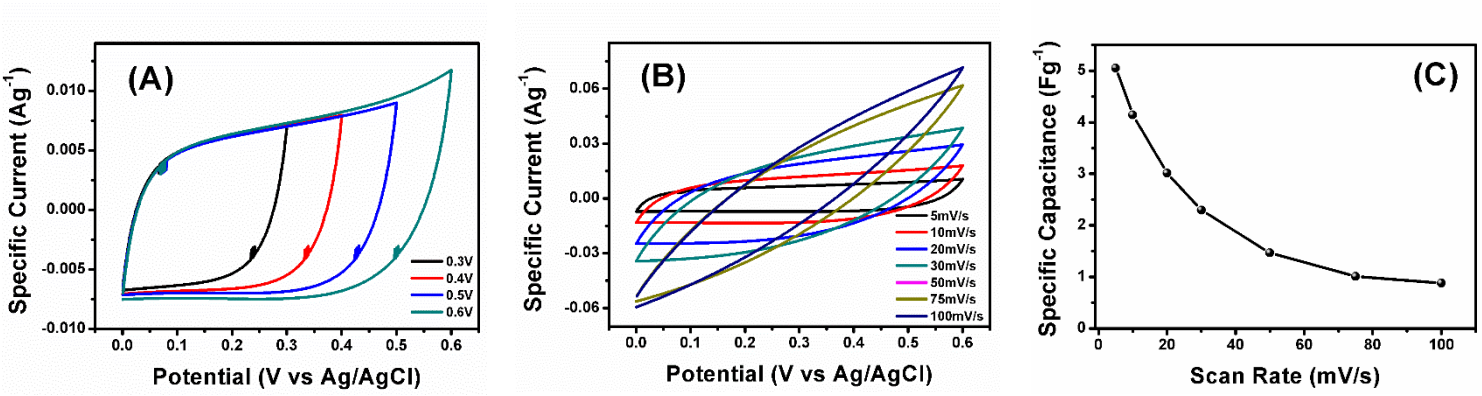

Figure 4.3: (A) CV of EDLC device utilizing electrolyte sample 1 at constant Scan rate of 5 mVs^{-1} (B) CV of EDLC device utilizing electrolyte 1 at constant potential of 0.6V (C) Variation of specific capacitance with scan rate for device with electrolyte sample 1

As the scan rate increasing (up to 100 mV s^{-1}), there seems to be deviation from the quasi-rectangular shape into a leaf-like shape, showing that the charge transfer resistance became the dominant factor in the device [7]. Figure 4.3(C) shows the variation of specific capacitance with scan rate for the device with electrolyte sample 1. The specific capacitances of device were

approximately 5.05, 4.15 , 3.01, 2.29, 1.47, 1.01 and 0.88 F g^{-1} measured at a scan rate from 5 , 10, 20, 30, 50, 75 and 100 mV s^{-1} respectively. The specific capacitance decreased as the scan rate increased indicating a capacitance retention of 17.42 % as the scan rate increases. This is because increasing the scan rate leads to a corresponding difficulty in the diffusion of electrolyte ions into the internal structure of electrodes and insufficient interaction between the electrolyte and materials of electrolyte thereby resulting in decrease of capacitance [7]–[9].

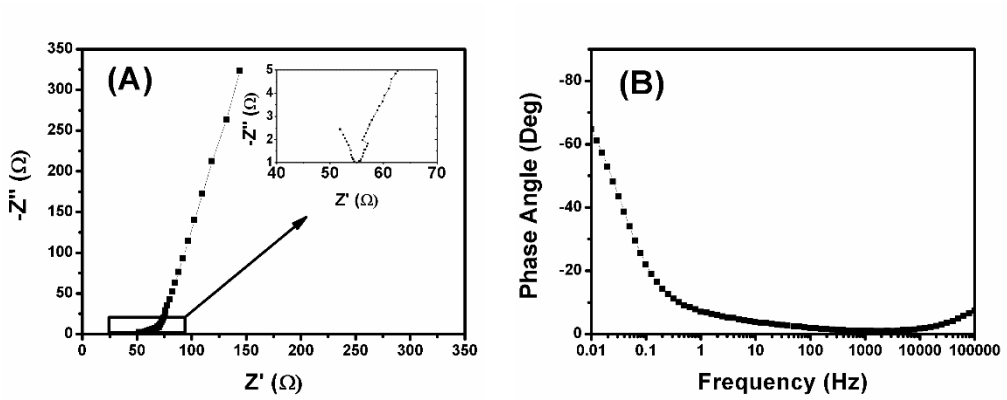

Figure 4. 4: (A) PEIS Nyquist plot of EDLC device utilizing electrolyte sample 1 (B) PEIS bode plot of EDLC device utilizing electrolyte sample 1

Figure 4.4(A) represents the PEIS Nyquist plot for a frequency range of 10 mHz to 100 kHz carried out on the EDLC using the as prepared electrolyte sample 1. The equivalent series resistance which is the intercept on the Z' was 55 Ω. Meanwhile, no semicircle was observed in either Nyquist plot, which implies the fast charge transfer process of the redox reaction at the electrode/electrolyte interface [10]. Figure 4.4(B) illustrates the PEIS bode plot of the device for a frequency range of 10 mHz to 100 kHz. The phase angle obtained is -64.6^0 which is somewhat distinct from -90^0 which is typical of ideal capacitors [11].

Figure 4.5(A) represents the cyclic voltammogram of the supercapacitor device utilizing electrolyte sample 2 (PEO + IL). The scan rate was kept constant at 50 mV s^{-1} and the potential was carefully varied from 0.5 V to 2 V. The maximum operating voltage of the device was 2V. As expected, figure 4.5(A) shows a quasi-rectangular shape, which shows that the produced electrodes exhibit the typical EDLCs behavior. Figure 4.5(B) represents the CV of the supercapacitor device utilizing electrolyte sample 2 at a constant potential of 2 V and varying scan rate from 5 mV s^{-1} to 100 mV s^{-1}. As the scan rate is increased (up to 100 mV s^{-1}), there seems to be a gradual deviation from the quasi-rectangular shape into a relatively greater area possessing leaf-like structure unlike that recorded for electrolyte sample 1 where the pear shape is sharper at both ends with a less area. Figure 4.5(C) shows the variation of specific capacitance with scan rate for the device with electrolyte sample 2. The specific capacitances of device were approximately 18.7, 16.1, 14.1, 12.9, 11.3, 10.5, and 9.7 F g^{-1} measured at a scan rate from 5, 10, 20, 30, 50, 75 and 100 mV s^{-1} respectively. The specific capacitance decreased as the scan rate increased indicating a capacitance retention of 51.9 % as the scan rate increases.

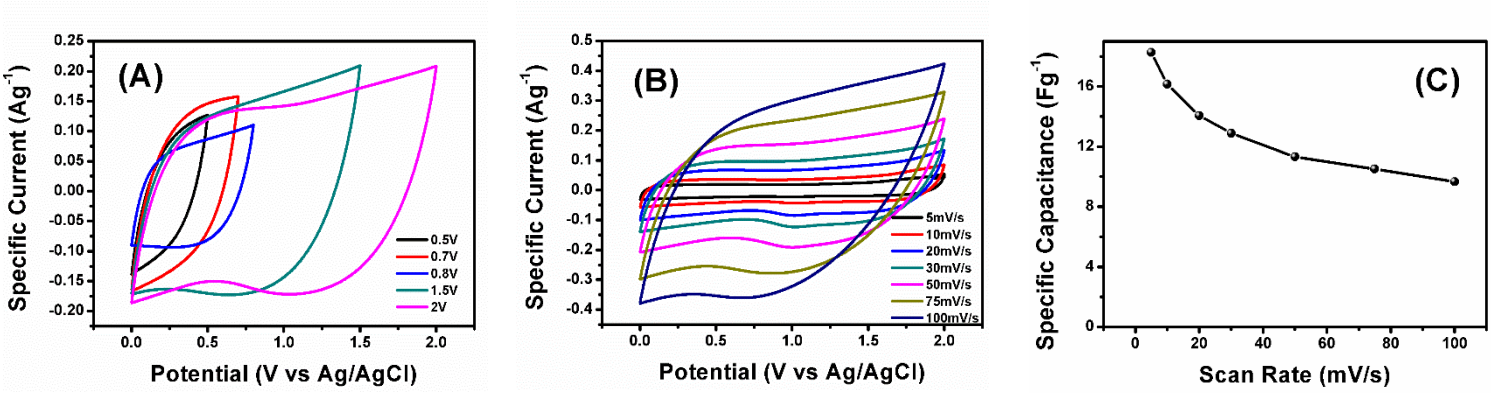

Figure 4. 5: (A) CV of an EDLC device utilizing electrolyte sample 2 at constant Scan rate of 50 mVs^{-1} (B) CV of EDLC device utilizing electrolyte 2 at constant potential of 2V (C) Variation of specific capacitance with scan rate for device with electrolyte sample 2

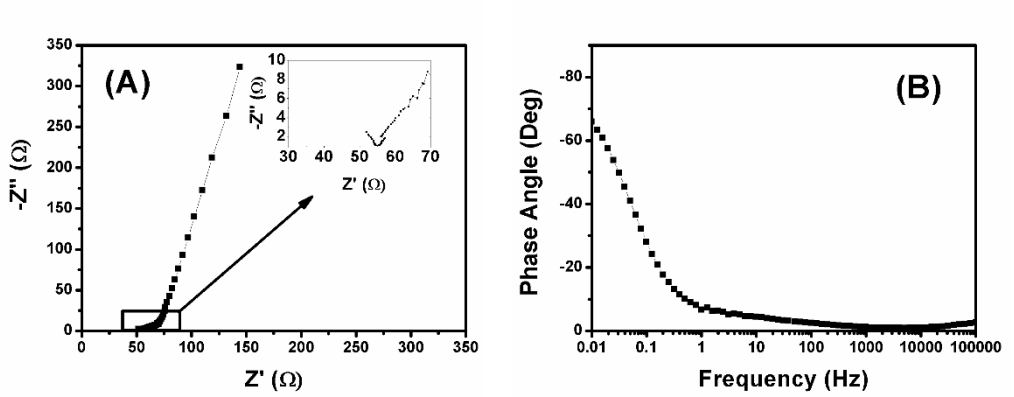

Figure 4. 6: (A) PEIS Nyquist plot of EDLC device utilizing electrolyte sample 2 (B) PEIS bode plot of EDLC device utilizing electrolyte sample 2

Figure 4.6(A) represents the PEIS Nyquist plot for a frequency range of 10 mHz to 100 kHz carried out on the EDLC using the as prepared electrolyte sample 2. The equivalent series resistance that is the intercept on the Z was 55 Ω which is the same as that of electrolyte sample 1. No semicirde was observed in either Nyquist plot, which still implies the fast charge transfer process of the redox reaction at the electrode/electrolyte interface. Figure 4.6(B) illustrates the PEIS bode plot of the device for a frequency range of 10 mHz to 100 kHz. The phase angle obtained is -65.9^0 which is slightly above that the EDLC device using electrolyte sample 1. The energy density of the device reached a maximum value of 5.07 Wh kg^{-1} at a specific capacitance of 18.3 Fg^{-1}. The highest power density attained by the device is 1.61 W kg^{-1} at a corresponding energy density of 3.14 Wh kg^{-1}.

Figure 4.7(A) represents the CV of the supercapacitor device utilizing electrolyte sample 3a (PEO + 0 wt. % IL + 10 wt. % $LiClO_4$). The scan rate was constant at 50 mV s^{-1} and the potential varied from 0.5 V to 1.2 V. The maximum operating voltage of the device was 1.2 V. A high voltage of 1.4 V was neglected as the maximum operating voltage of the device because at this voltage, degradation through redox reaction must have occurred. Figure 4.7(B) represents the cyclic voltammogram of the EDLC device utilizing electrolyte sample 3a at a constant potential of 1.2 V and varying scan rate from 5 mV s^{-1} to 100mV s^{-1}. The CV curves with a maximum potential window of 1.2 V of the EDLC at different scan rates showed quasi-rectangular shapes, which is similar with other electrolyte samples. As the scan rate is increased (up to 100 mV s^{-1}), a change from the

quasi-rectangular shape to a leaf-like shape occurs. Figure 4.7(C) shows the variation of specific capacitance with scan rate for the device with electrolyte sample 3a. The specific capacitances of device were approximately 15.8, 15.4, 14.4, 12.4, 10.5, 8.8 and 7.5 F g^{-1} measured at a scan rate from 5, 10, 20, 30, 50, 75 and 100 mV s^{-1} respectively. The specific capacitance decreased as the scan rate increased indicating a capacitance retention of 47.5 % as the scan rate increases.

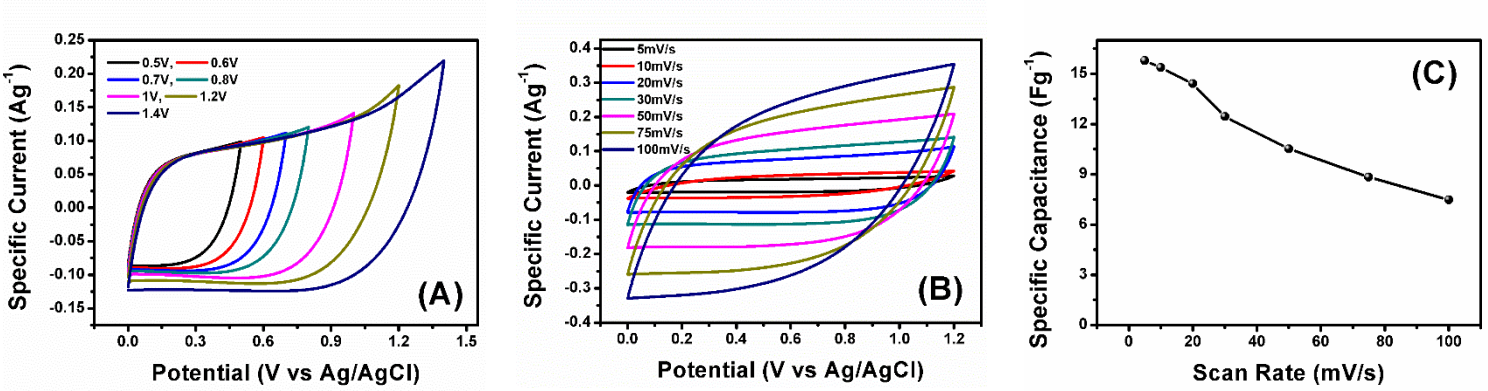

Figure 4.7: (A) CV of EDLC device utilizing electrolyte sample 3a at constant scan rate of 50 mVs $^{-1}$ (B) CV of EDLC device utilizing electrolyte 3a at constant potential of 1.2V (C) Variation of specific capacitance with scan rate for device with electrolyte sample 3a

Figure 4.8(A) represents the PEIS Nyquist plot for a frequency range of 10 mHz to 100 kHz carried out on the EDLC using the as prepared electrolyte sample 3a. The equivalent series resistance, which is the intercept on the Z-axis, was 27 Ω, which is quite different from that recorded for the devices using electrolyte sample 1 and 2. As with the previous cases, no semicircle was observed in the Nyquist plot, which still implies the fast charge transfer process of the redox reaction at the electrode/electrolyte interface. Figure 4.8(B) illustrates the PEIS bode plot of the device for a frequency range of 10 mHz to 100 k Hz. The phase angle obtained is -76.8 ^{0} which is significantly greater than the previous two tested devices. The energy density of the device reached a maximum value of 0.95 Wh kg^{-1} at a specific capacitance of 15.8 Fg^{-1}. The highest power density attained by the device is 1.4 W kg^{-1} at a corresponding energy density of 0.81 Wh kg^{-1}.

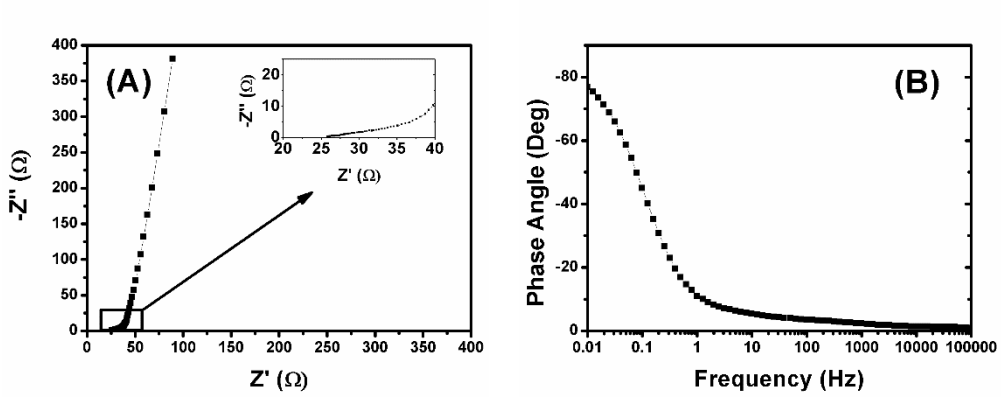

Figure 4.8: (A) PEIS Nyquist plot of EDLC device utilizing electrolyte sample 3a (B) PEIS bode plot of EDLC device utilizing electrolyte sample 3a

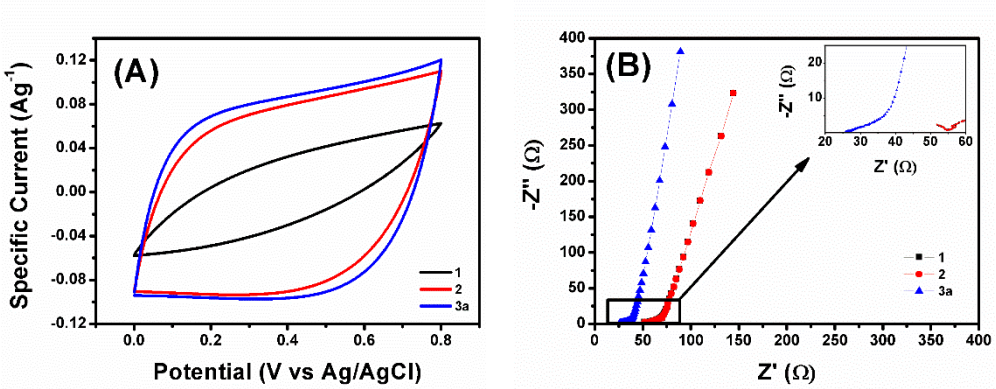

Figure 4.9: (A) Comparison of the CV of EDLC devices utilizing electrolyte samples 1, 2 and 3a at a potential of 0.8V and scan rate of 50 mVs^{-1} (B) Comparison of the PEIS Nyquist plots of EDLC devices utilizing electrolyte samples 1, 2 and 3a

Figure 4.9(A) delineates the comparison of the CV of the EDLC devices employing electrolyte samples 1, 2 and 3a. The area of the curve under the CV represents the charge stored by the device. The EDLC device using electrolyte sample 3a stores charge slightly more than that utilizing 2. The device employing electrolyte sample 1 stores the least charge and as such is unsuitable for further consideration. Figure 4.9(B) represents the comparison of the PEIS Nyquist plots of the

EDLC devices utilizing electrolyte samples 1, 2 and 3a. The EDLC device using electrolyte sample 3a obviously has the best equivalent series resistance of 27 Ω in comparison to that of the devices using electrolyte samples 1, 2 and 3 as determined from the Z-axis. Since the equivalent series resistance is inversely proportional to the power density, a lower value of resistance implies maximize the power density. Also the EDLC which employs electrolyte sample 3a, is more stable than that using electrolyte samples 1 and 2 as its phase angle is -76.8^0.

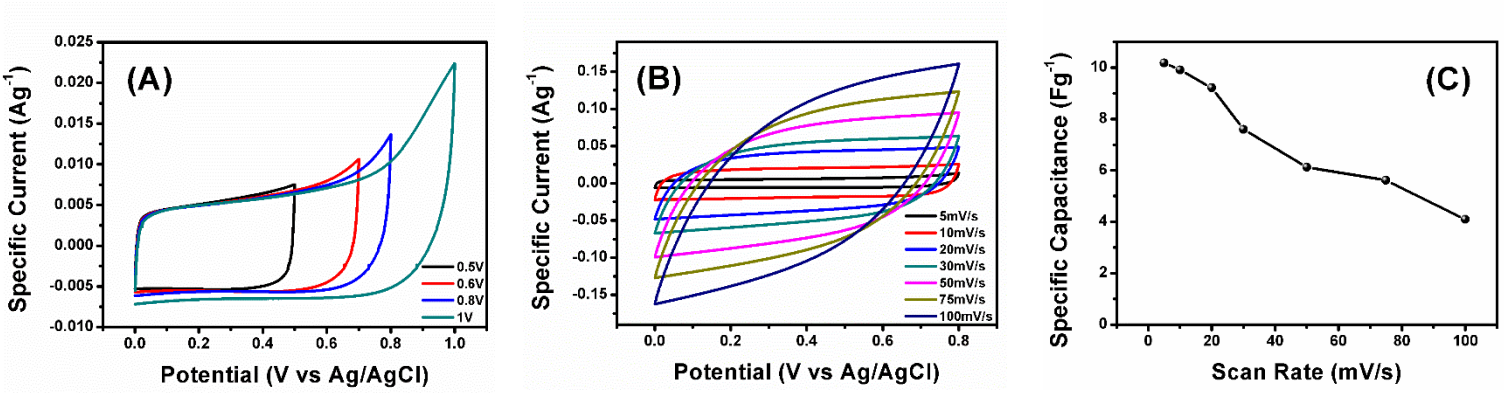

Figure 4.10: (A) CV of EDLC device utilizing electrolyte sample 3b at constant scan rate of 5mVs^{-1} (B) CV of EDLC device utilizing electrolyte 3b at constant potential of 0.8V (C) Variation of specific capacitance with scan rate for device with electrolyte sample 3b

Figure 4.10(A) represents the CV of the supercapacitor device utilizing electrolyte sample 3b (PEO + 5 wt. % IL + 10 wt. % $LiClO_4$). The scan rate was kept constant at 5 mV s^{-1} and the potential was carefully varied from 0.5 V to 1 V. The maximum operating voltage of the device 0.8 V. A high voltage of 1 V was neglected as the maximum operating voltage of the device because at this voltage, degradation through redox reaction must have occurred. Figure 4.10(B) represents the CV of the EDLC device utilizing electrolyte sample 3b at a constant potential of 0.8 V and varying scan rate from 5 mV s^{-1} to 100 mV s^{-1}. The CV curves with a maximum potential window of 0.8 V of the EDLC at different scan rates showed quasi-rectangular shapes, which is similar with other electrolyte samples. As the scan rate is increased (up to 100 mV s^{-1}), a change from the quasi-rectangular shape to a leaf-like shape occurs. Figure 4.10(C) shows the variation of specific

capacitance with scan rate for the device with electrolyte sample 3b. The specific capacitances of device were approximately 10.2, 9.9, 9.2, 7.6, 6.1, 5.6 and 4.1 F g^{-1} measured at a scan rate from 5, 10, 20, 30, 50, 75 and 100 mV s^{-1} respectively. The specific capacitance decreased as the scan rate increased indicating a capacitance retention of 40.2% as the scan rate increases.

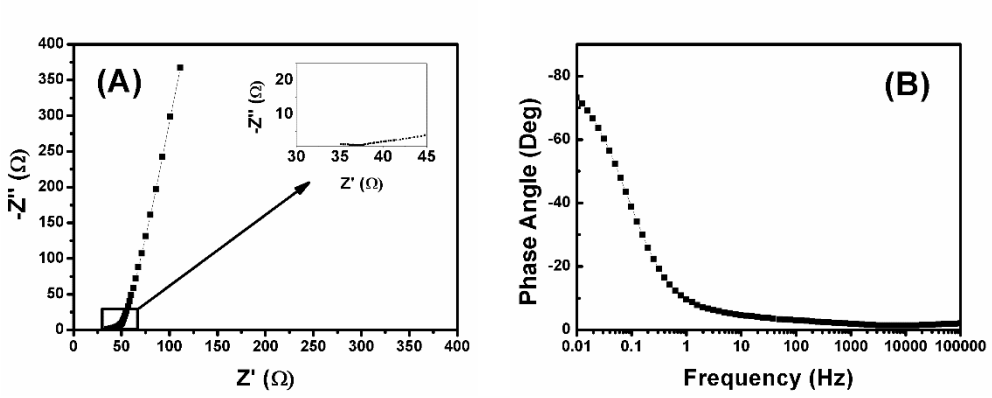

Figure 4.11: (A) PEIS Nyquist plot of EDLC device utilizing electrolyte sample 3b (B) PEIS bode plot of EDLC device utilizing electrolyte sample 3b

Figure 4.11(A) represents the PEIS Nyquist plot for a frequency range of 10 mHz to 100 kHz carried out on the EDLC device using the as prepared electrolyte sample 3b. The equivalent series resistance, which is the intercept on the Z-axis, 37 Ω. As with the previous cases, no semicirde was observed in the Nyquist plot, which still implies the fast charge transfer process of the redox reaction at the electrode/electrolyte interface. Figure 4.11(B) illustrates the PEIS bode plot of the device for a frequency range of 10 mHz to 100 kHz. The phase angle obtained is -73.3^0. The energy density of the device reached a maximum value of 0.18 Wh kg^{-1} at a specific capacitance of 10.2 Fg^{-1}. The highest power density attained by the device is 0.32 W kg^{-1} at a corresponding energy density of 0.22 Wh kg^{-1}.

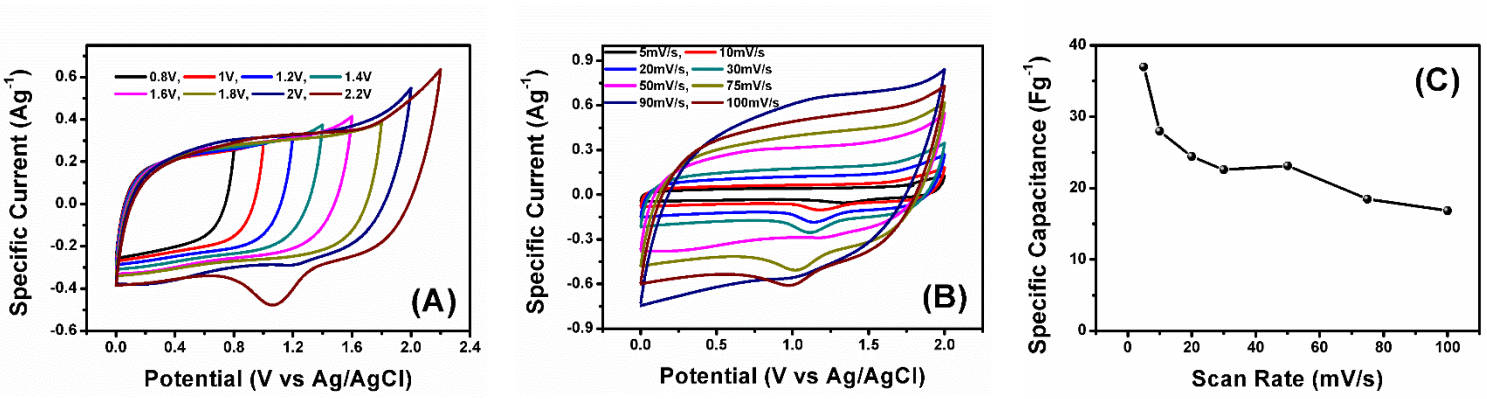

Figure 4. 12: (A) CV of EDLC device utilizing electrolyte sample 3d at constant scan rate of 40mVs^{-1} (B) CV of EDLC device utilizing electrolyte 3d at constant potential of 1V (C) Variation of specific capacitance with scan rate for device with electrolyte sample 3d

Figure 4.12(A) represents the cyclic voltammogram of the supercapacitor device utilizing electrolyte sample 3d (PEO + 15 wt. % IL + 10 wt. % $LiClO_4$). The scan rate was constant at 40 mV s^{-1} and the potential was varied from 0.5 V to 2. 2 V. The maximum operating voltage of the device was 2 V. A high voltage of 2.2 V was neglected as the maximum operating voltage of the device to preclude a degradation of the device through redox reaction. Figure 4.12(B) represents the cyclic voltammogram of the EDLC device utilizing electrolyte sample 3d at a constant potential of 2 V and varying scan rate from 5 mV s^{-1} to 100 mV s^{-1}. The CV curves with a maximum potential window of 2 V of the EDLC at different scan rates showed quasi-rectangular shapes which is similar with other electrolyte samples. As the scan rate is increased (up to 100 mV s^{-1}), a change from the quasi-rectangular shape to a leaf-like shape occurs. Figure 4.12(C) shows the variation of specific capacitance with scan rate for the device with electrolyte sample 3b. The specific capacitances of device were approximately 36.9, 27.8, 24.4, 22.6, 23.1, 18.5 and 16.8 F g^{-1} measured at a scan rate from 5, 10, 20, 30, 50, 75 and 100 mV s^{-1} respectively. The specific capacitance decreased as the scan rate increased indicating a capacitance retention of 45.5 % as the scan rate increases

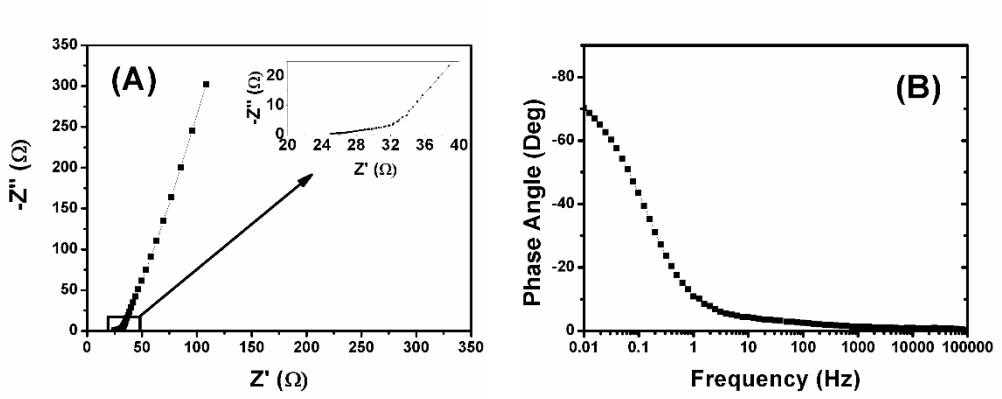

Figure 4. 13: (A) PEIS Nyquist plot of EDLC device utilizing electrolyte sample 3d (B) PEIS bode plot of EDLC device utilizing electrolyte sample 3d

Figure 4.13(A) represents the PEIS Nyquist plot for a frequency range of 10 mHz to 100 kHz carried out on the EDLC device using the as prepared electrolyte sample 3d. The equivalent series resistance, which is the intercept on the Z-axis, 27 Ω. As with the previous cases, no semicirde was observed in the Nyquist plot, which still implies the fast charge transfer process of the redox reaction at the electrode/electrolyte interface. Figure 4.13(B) illustrates the PEIS bode plot of the device for a frequency range of 10 mHz to 100 kHz. The phase angle obtained is -70^0. At a specific capacitance of 37 Fg^{-1}. The highest power density attained by the device is 5.6 W kg^{-1} at a corresponding energy density of 8.9 Wh kg^{-1}.

Figure 4.14(A) represents the CV of the supercapacitor device utilizing electrolyte sample 3e (PEO + 20 wt. % IL + 10 wt. % $LiClO_4$). The scan rate was constant at 50 mV s^{-1} and the potential was carefully varied from 0.8 V to 2.3 V. The maximum operating voltage of the device was found to be 2.3 V. Figure 4.14(B) represents the CV of the EDLC device utilizing electrolyte sample 3e at a constant potential of 2.3V and varying scan rate from 5mV s^{-1} to 100mV s^{-1}. The CV curves with a maximum potential window of 2.3 V of the EDLC at different scan rates showed quasi-rectangular shapes, which is similar with other electrolyte samples. As the scan rate is increased (up to 100 mV s^{-1}), a change from the quasi-rectangular shape to a leaf-like shape occurs. Figure 4.14(C) shows the variation of specific capacitance with scan rate for the device with electrolyte sample

3e. The specific capacitances of device were approximately 54.9, 41.8, 35.1, 32.8, 30.4, 27.8 and 26 F g^{-1} measured at a scan rate from 5, 10, 20, 30, 50, 75 and 100 mV s^{-1} respectively. The specific capacitance decreased as the scan rate increased indicating a capacitance retention of 47.3 % as the scan rate increases.

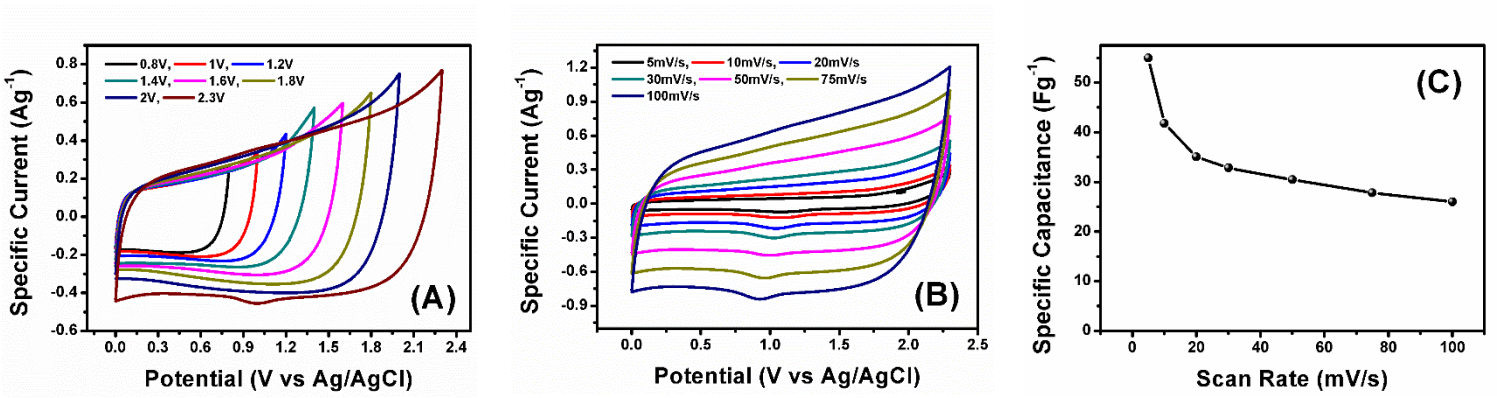

Figure 4. 14: (A) CV of EDLC device utilizing electrolyte sample 3e at constant scan rate of 40mV s^{-1} (B) CV of EDLC device utilizing electrolyte 3e at constant potential of 1V (C) Variation of specific capacitance with scan rate for device with electrolyte sample 3e

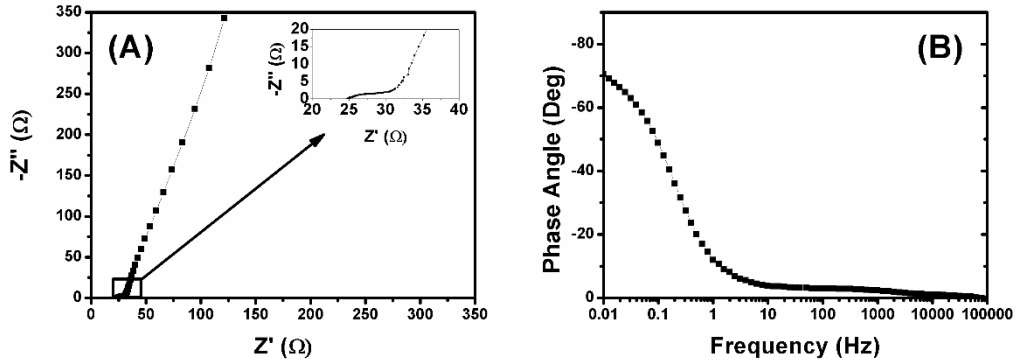

Figure 4. 15: (A) PEIS Nyquist plot of EDLC device utilizing electrolyte sample 3e (B) PEIS bode plot of EDLC device utilizing electrolyte sample 3e

Figure 4.15(A) represents the PEIS Nyquist plot for a frequency range of 10 mHz to 100 kHz carried out on the EDLC device using the as prepared electrolyte sample 3e. The equivalent series resistance, which is the intercept on the Z-axis 26 Ω. As with the previous cases, no semicircle was observed in the Nyquist plot, which still implies the fast charge transfer process of the redox reaction at the electrode/electrolyte interface. Figure 4.15(B) illustrates the PEIS bode plot of the device for a frequency range of 10 mHz to 100 kHz. The phase angle obtained is -70.4^{0}. The energy density of the device reached a maximum value of 23.2 Wh kg^{-1} at a specific capacitance of 55 Fg^{-1}. The highest power density attained by the device is 10.8 W kg^{-1} at a corresponding energy density of 13 Wh kg^{-1}.

REFERENCES

[1] O. Kim, S. Y. Kim, H. Ahn, C. W. Kim, Y. M. Rhee, and M. J. Park, "Phase behavior and conductivity of sulfonated block copolymers containing heterocyclic diazole-based ionic liquids," Macromolecules, vol. 45, no. 21, pp. 8702–8713, 2012.

[2] A. Chandra, P. K. Singh, and S. Chandra, "Semiconductor-dispersed polymer electrolyte composites," Solid State Ionics, vol. 154–155, no. October 2018, pp. 15–20, 2002.

[3] L. Berkeley and K. City, "ITll Lawrence Berkeley · Laboratory," 2011.

[4] S. K. Chaurasia, R. K. Singh, and S. Chandra, "Dielectric relaxation and conductivity studies on (PEO:$LiClO_4$) polymer electrolyte with added ionic liquid [BMIM][PF_6]: Evidence of ion-ion interaction," J. Polym. Sci. Part B Polym. Phys., vol. 49, no. 4, pp. 291–300, 2011.

[5] H. J. Woo, S. R. Majid, and A. K. Arof, " Transference number and structural analysis of proton conducting polymer electrolyte based on poly(ϵ -caprolactone) ," Mater. Res. Innov., vol. 15, no. sup2, pp. s49–s54, 2011.

[6] N. Elgrishi, K. J. Rountree, B. D. McCarthy, E. S. Rountree, T. T. Eisenhart, and J. L. Dempsey, "A Practical Beginner's Guide to Cyclic Voltammetry," J. Chem. Educ., vol. 95, no. 2, pp. 197–206, 2018.

[7] H. Yang, Y. Liu, L. Kong, L. Kang, and F. Ran, "Biopolymer-based carboxylated chitosan hydrogel film crosslinked by HCl as gel polymer electrolyte for all-solid-sate supercapacitors," J. Power Sources, vol. 426, no. March, pp. 47–54, 2019.

[8] V. Subramanian, C. Luo, A. M. Stephan, K. S. Nahm, S. Thomas, and B. Wei, "Supercapacitors from activated carbon derived from banana fibers," J. Phys. Chem. C, vol. 111, no. 20, pp. 7527–7531, 2007.

[9] D. Wang, L. Yu, B. He, and L. Wang, "A high-performance carbon-carbon(C/C) quasi-solid-state supercapacitor with conducting gel electrolyte," Int. J. Electrochem. Sci., vol. 13, no.

3, pp. 2530–2543, 2018.

[10] J. Park, Y. E. Yoo, L. Mai, and W. Kim, “Rational Design of a Redox-Active Nonaqueous Electrolyte for a High-Energy-Density Supercapacitor Based on Carbon Nanotubes,” ACS Sustain. Chem. Eng., vol. 7, no. 8, pp. 7728–7735, 2019.

[11] F. O. Ochai-Ejeh et al., “High electrochemical performance of hierarchical porous activated carbon derived from lightweight cork (Quercus suber),” J. Mater. Sci., vol. 52, no. 17, pp. 10600–10613, 2017.

CHAPTER FIVE

CONCLUSION AND RECOMMENDATION(S)

5.1 Conclusion

This project work has demonstrated a facile way to enhance the energy density of EDLC devices, through the application gel polymer based electrolyte. The use of additives such as ionic liquid and conducting salts with the gel electrolyte, improved the energy density of the supercapacitor when compared to aqueous electrolyte. The gel polymer electrolyte is based on methanol, polyethylene oxide (PEO), lithium perchlorate ($LiClO_4$) and ionic liquid (IL), tetraethylammonium tetrafluoroborate ($TEABF_4$). Polymer electrolyte films of 7 different compositions were prepared which are: pristine PEO (1), PEO:10 wt. % IL (2), PEO:10 wt.% $LiClO_4$ (3a), PEO:10 wt. % $LiClO_4$ + 5 wt. % IL (3b), PEO: 10 wt. % $LiClO_4$ + 10 wt. % IL (3c), PEO:10 wt. % $LiClO_4$ + 15 wt. % IL (3d) and PEO:10 wt. % $LiClO_4$ + 20 wt. % IL (3e). Supercapacitor devices were assembled using the as prepared gel polymer electrolytes and electrodes made from graphite (active carbon), chitosan based binder and conducting carbon addictive. The devices made with electrolyte samples 3d and 3e exhibited the most outstanding electrochemical performance. The device made with electrolyte specimen 3d showed a maximum operating voltage window of 2 V, a peak capacitance of 36.9 F g^{-1}, maximum energy density of 10.3 kWh g^{-1} and a power density of 5.6 kW/g. The device made with electrolyte specimen 3e showed a maximum operating voltage window of 2.3 V, a peak capacitance of 54.9 Fg^{-1}, maximum energy density of 23.2 kWh g^{-1} and a power density of 10.8 kW/g. Furthermore, the phase angles for the device made with electrolyte sample 3d was -70.0^0 while that for the device made with electrolyte sample 3e was -70.4^0; these values are close to the capacitive ideal of -90^0. Indeed, gel polymer electrolytes can conveniently serve as an alternative for the readily used aqueous and ionic liquid electrolytes for improved electrochemical capacitor applications.

5.2 Recommendation(s)

The scope of this work was to exploring the potential of a PEO-polymer blend electrolyte as an alternative to aqueous and ionic liquid electrolytes for electrochemical supercapacitor applications. In the process of characterization of the PEO-polymer blend electrolyte, only the FTIR was employed. Further characterization can be carried out via techniques such as x-ray diffraction (XRD) to understand the structural composition and crystalline nature of the electrolyte material, scanning electron microscopy (SEM) to comprehend the microstructural configuration of the electrolyte material, differential scanning calorimetry (DSC) to ascertain the thermal stability of the material and to determine the operating temperature range. In addition, further electrochemical characterization could be done via the galvanostatic charge/discharge technique so as to determine its cyclability and also to have an idea of its suitability in real time. Furthermore, optimization should be carried out to expand the operating voltage window of the device. This is achievable by varying the proportions/ratios of the constituents of the electrolytes (PEO, $LiClO_4$, and IL). The effect of this is that more room would be available for the increment of the capacitance and energy density value of the device. Generally, even though high power densities are attainable with polymer electrolytes, the equivalent series resistance of EDLCs employing gel polymer electrolytes are still on the high side as evident in literature. Attempts and further research could be geared towards the reduction of the ESR of the EDLC device to yield greater power density.